Holographic coarse-grained states and the necessity of perfect entanglement

Yi-Yu Lin[1,2,*] and Jun Zhang[3,†]

[1]*Beijing Institute of Mathematical Sciences and Applications (BIMSA), Beijing 101408, China*
[2]*Yau Mathematical Sciences Center (YMSC), Tsinghua University, Beijing 100084, China*
[3]*Department of Physics and Astronomy, University of Alabama, 514 University Boulevard, Tuscaloosa, Alabama 35487, USA*

(Received 12 February 2024; accepted 17 May 2024; published 13 June 2024)

In the framework of the holographic principle, focusing on a central concept, conditional mutual information, we construct a class of coarse-grained states, which are intuitively connected to a family of thread configurations. These coarse-grained states characterize the entanglement structure of holographic systems at a coarse-grained level. Importantly, these coarse-grained states can be used to further reveal nontrivial requirements for the holographic entanglement structure. Specifically, we employ these coarse-grained states to probe the entanglement entropies of disconnected regions and the entanglement wedge cross section dual to the inherent correlation in a bipartite mixed state. The investigations demonstrate the necessity of perfect tensor state entanglement. Moreover, in a certain sense, our work establishes the equivalence between the holographic entanglement of purification and the holographic balanced partial entropy. We also construct a thread configuration with the multiscale entanglement renormalization ansatz (MERA) structure, reexamining the connection between the MERA structure and kinematic space.

DOI: 10.1103/PhysRevD.109.126012

I. INTRODUCTION

In the framework of holographic duality [1–3], the Ryu-Takayanagi (RT) formula [4–6] for holographic entanglement entropy suggests a profound connection between gravity and quantum entanglement. The formula states that the entanglement entropy $S(A)$ of a subsystem A in the holographic quantum system can be precisely calculated by the area of a minimal extremal surface γ_A in the dual higher-dimensional spacetime,

$$S_A = \frac{\mathrm{Area}(\gamma_A)}{4G_N}, \tag{1}$$

where γ_A is homologous to A and completely separating A from B.

Following this clue, tensor networks have proven useful for studying the entanglement structure in holographic gravity [7–24].[1] This tool was initially employed in the intersection of condensed matter physics and quantum information theory to characterize a series of states (especially ground states) of quantum many-body systems. Essentially, they describe a class of states that can be represented as a contraction of many small tensors. Each small tensor is graphically represented as a subdiagram with legs extending from a vertex, while tensor contractions are represented by connections between legs of different subdiagrams. Finally, these subdiagrams are connected into a network pattern, known as a tensor network. Our research is interested in characterizing the entanglement structure of holographic gravity from a complementary perspective—the "thread" perspective [53–63]. Similarly, the thread perspective is also geometrically intuitive. The difference is that, in the tensor network picture, the objects of interest are tensors represented by local subdiagrams, while in the thread perspective, the objects of interest are threads with global features. Broadly speaking, we can define a thread configuration as a collection of threads, wherein the end points of the threads are anchored in the boundary quantum system. This perspective is inspired by the so-called bit threads [53–56],[2] which arise from the rephrasing of the RT formula for holographic entanglement entropy.

In a series of previous works [59–63], we constructed a class of thread configurations closely related to many concepts in the research of holographic duality, such as bit threads [53–56], kinematic space [41,87], holographic entropy cone [88–91], and holographic partial

*yiyu@bimsa.cn
†jzhang163@crimson.ua.edu

[1]For more research on tensor networks in the holographic context, see, e.g., [25–52].

[2]For the recent developments of bit threads see, e.g., [57–86].

entanglement entropy [59,64,92–96]. These connections are somewhat natural and easily obtained. Especially, the conditional mutual information (CMI), which characterizes the density of entanglement entropy in some sense, plays a central role in all these themes. Discussions about these connections can be found in a series of papers [59–65]. However, our main point is that these thread configurations can be endowed with a clear interpretation of a class of quantum states. From now on, we will systematically refer to them as coarse-grained states.[3] As the name suggests, coarse-grained states are expected to only characterize the quantum entanglement of holographic quantum systems at a coarse-grained level. The true entanglement structure of a holographic quantum system is expected to be much more complex. The key point is that the study of these coarse-grained states will lead us to recognize the necessity of perfect tensor entanglement in holographic quantum systems. A preliminary discussion can be found in [63].

In this paper, by using these coarse-grained states to further characterize some of the geometric duals of quantum information theory quantities, such as the RT surface corresponding to the entanglement entropy of disconnected regions and the entanglement wedge cross section (EWCS) corresponding to the entanglement of purification (EoP) [97,98], we find that, even at the coarse-grained level, we encounter unavoidable difficulties. Our core idea is that the introduction of perfect tensor entanglement [12] naturally resolves these issues. The introduction of perfect entanglement not only achieves the characterization of the entanglement entropies of disconnected regions [63], but also naturally gives rise to the equivalence between two quantum information theory quantities related to the entanglement wedge cross section—the entanglement of purification [97,98] and the balanced partial entropy (BPE) [99–101]. In other words, it allows the so-called BPE to reasonably characterize the inherent correlation in a bipartite mixed state. Moreover, to demonstrate our ideas more clearly and concretely, we construct a thread configuration with a multiscale entanglement renormalization ansatz (MERA) structure [7–11] and associate it with a coarse-grained state characterized by perfect tensor entanglement. We further explore the connection between the MERA structure and kinematic space [41,87]. The construction also has an inspiring role in understanding the relationship between MERA tensor networks and bit threads [71].

The structure of this paper is as follows: In Sec. II, we provide a review of refined thread configurations, coarse-grained states, and the thread-state correspondence. In Sec. III, motivated by the thread perspective for characterizing the entanglement entropy of disconnected regions and the entanglement wedge cross section, we propose the necessity of introducing perfect tensor entanglement. In Sec. IV, we construct a thread configuration with the MERA structure and its corresponding coarse-grained state to illustrate our proposal. This thread configuration provides an example of thread-state correspondence and is closely related to kinematic space. In Secs. V and VI, we interconnect all intersecting threads in the MERA-structure thread configuration to introduce the perfect tensor entanglement and demonstrate that it can nicely solve the problems proposed in Sec. III. Section VII concludes the paper with discussions.

II. BACKGROUND REVIEW

A. Refined thread configurations

A naive illustration of the entanglement structure revealed by the RT formula is shown in Fig. 1(a). Consider the entanglement entropy of a subsystem A and its complement B in a pure state of a CFT dual to a pure AdS space. We can envision a family of uninterrupted threads connecting A and its complement B, passing through the RT surface γ_A. The number of these threads, denoted as N_{AB}, is exactly equal to the entanglement entropy $S(A)$ between A and B:

$$N_{AB} = S_A. \tag{2}$$

These threads are commonly referred to as "bit threads" [53–56].

We can do better. We can construct a series of increasingly refined thread configurations that can be used to calculate the entanglement entropies for more than one region [57–59,61,62]. As shown in Fig. 1(b), we can further decompose region A into $A = A_1 \cup A_2$ and B into $B = A_3 \cup A_4$. Thus, we can construct a more refined thread configuration that can calculate the entanglement entropies between six connected regions and their complements, including A_1, A_2, A_3, A_4, $A = A_1 \cup A_2$, and $A_2 \cup A_3$. In other words, the number of threads connecting these six regions and their complements is exactly equal to the corresponding entanglement entropy. Similarly, we can further divide the quantum system M into more adjacent and nonoverlapping basic regions $A_1, A_2, ..., A_N$ and then obtain corresponding more refined thread configurations [see Fig. 1(c)].[4] This process can be iterated (as long as each basic region is still much larger than the Planck length to ensure the applicability of the RT formula). Here, we define basic regions such that

[3] In previous literature, we often referred to them as distilled states, given their close connection with entanglement distillation tensor networks [58].

[4] These thread configurations are referred to as "locking" thread configurations in the literature [57]. Note that here we have carefully drawn the threads to appear perpendicular to the RT surfaces they pass through, in keeping with the conventional property of bit threads. However, in the sense of coarse-grained states, only the topology is really important, and we have not yet seriously considered the exact trajectories of these threads.

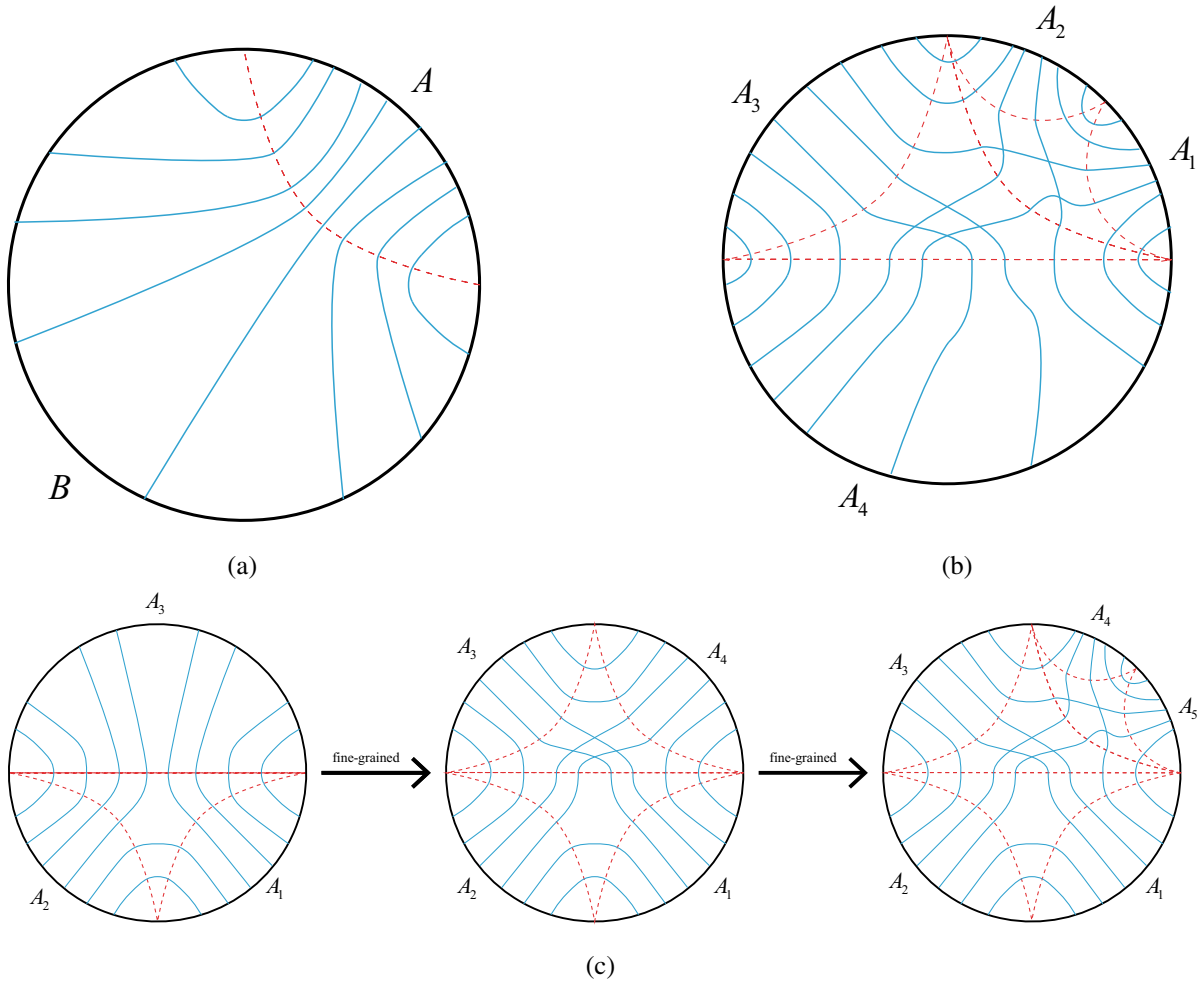

FIG. 1. (a) A thread picture characterizing the entanglement entropy between two complementary regions. (b) A more refined thread configuration characterizing a set of entanglement entropies involving more subregions. (c) By iteratively dividing the quantum system, more and more refined thread configurations can be constructed, characterizing the entanglement structure at more and more refined levels, see details in [61]. Here the threads are schematically represented as blue lines, and the RT surfaces are represented as red dashed lines.

$$A_i \cap A_j = \varnothing, \qquad \bigcup A_i = M. \tag{3}$$

Next, we can define a function $N_{ij} \equiv N_{A_i \leftrightarrow A_j}$ for each pair of basic regions A_i and A_j, representing the number of threads connecting A_i and A_j. The papers [59,61,62] impose the following physical requirement on the thread configuration: the set of threads $\{N_{ij}\}$ should satisfy

$$S_{a(a+1)\ldots b} = \sum_{i,j} N_{ij}, \quad \text{where } i \in \{a, a+1, \ldots, b\}, \quad j \notin \{a, a+1, \ldots, b\}. \tag{4}$$

Here, $S_{a(a+1)\ldots b}$ represents the entanglement entropy S_A of a connected composite region $A = A_{a(a+1)\ldots b} \equiv A_a \cup A_{a+1} \cup \ldots \cup A_b$. This equation can be intuitively understood as the entanglement entropy between A and its complement $\bar{A}$ coming from the sum of N_{ij} between basic regions A_i within A and basic regions A_j within the complement $\bar{A}$. Thread configurations satisfying condition (4) are commonly referred to as locking thread configurations, borrowing terminology from network flow theory. Solving condition (4), the first thing we find is that the number of threads connecting two basic regions is precisely given by the so-called conditional mutual information. In other words, the conditional mutual information characterizes the correlation between two regions A_i and A_j separated by a distance L,

$$\begin{aligned} N_{A_i \leftrightarrow A_j} &= \frac{1}{2} I(A_i, A_j | L) \\ &\equiv \frac{1}{2}\big[S(A_i \cup L) + S(A_j \cup L) \\ &\quad - S(A_i \cup L \cup A_j) - S(L)\big]. \end{aligned} \tag{5}$$

Here, $L = A_{(i+1)\ldots(j-1)}$ represents the region between A_i and A_j, which is a composite region consisting of many basic regions and also represents the distance between A_i and A_j.

In fact, this class of refined thread configurations is closely related to various concepts proposed from different perspectives in holographic duality research, including kinematic space [41,87], entropy cone [88–91], and holographic partial entanglement entropy [59,64,92–96]. These connections are, in a sense, natural and easy to obtain, especially where the conditional mutual information plays a central role. For example, it is defined as the volume measure in kinematic space [41,87], characterizing the density of entanglement entropy. Discussions about these connections can be found in a series of articles [59–65]. The key point is that, in our framework, we will understand these refined thread configurations as a kind of coarse-grained state of the holographic quantum system [61–63], which only characterizes the entanglement structure of the holographic quantum system at a coarse-grained level. Our approach is to explore the properties that these entanglement structures should have by studying them at this level.

B. Coarse-grained state

Now, we will refer to these thread configurations as representing the coarse-grained state of the holographic quantum system. In [61–63], this is also referred to as thread-state correspondence. In simple terms, the idea is that, in such a locking thread configuration, each thread can be understood as a pair of maximally entangled qudits. One end of the thread corresponds to one qudit. For example, let us take $d = 2$, so one end of the thread corresponds to a qubit. Thus, a thread corresponds to

$$|\text{thread}\rangle = \frac{1}{\sqrt{2}}(|00\rangle + |11\rangle). \tag{6}$$

Then the direct product of the states of all threads in the thread configuration gives a coarse-grained state of the quantum system,

$$|\Psi\rangle_{\text{coarse}} = \prod_{\text{all thread}} |\text{thread}\rangle. \tag{7}$$

Refs. [61–63] argue that, if we take the partial trace of the coarse-grained state $|\Psi\rangle_{\text{coarse}}$ to obtain reduced density matrices for various connected regions $\{A_i, A_iA_{i+1}, A_iA_{i+1}A_{i+2}, \ldots\}$ and calculate the corresponding von Neumann entropies, we exactly obtain a set of correct holographic entanglement entropies.

In fact, the idea of thread-state correspondence expresses more than what expression (6) presents. By combining with the surface/state duality [21,22] or tensor network models, each thread actually represents not only the entanglement between the two end points of the thread, but also the entanglement between all degrees of freedom that the thread passes through in the holographic bulk. For this, we can agree on a thread-state rule: each thread is in a state [61–63]

$$|\text{thread}\rangle = \frac{1}{\sqrt{2}}(|\text{red}\rangle + |\text{blue}\rangle). \tag{8}$$

Then, the entanglement between multiple sites (or qudits) strung together by a single thread follows the rules: each $|\text{red}\rangle$ state actually represents that the qudits the thread passes through are all in their own $|0\rangle$ state, and each $|\text{blue}\rangle$ state actually represents that the qudits the thread passes through are in their own $|1\rangle$ state, that is,

$$\begin{aligned} |\text{red}\rangle &= |0_1 0_2 \cdots 0_n\rangle, \\ |\text{blue}\rangle &= |1_1 1_2 \cdots 1_n\rangle. \end{aligned} \tag{9}$$

In fact, we will see explicit examples of this interpretation in the following sections.

III. MOTIVATION AND PROPOSAL: NECESSITY OF PERFECT ENTANGLEMENT

As the name suggests, the coarse-grained state is just a characterization of quantum entanglement at the coarse-grained level of the holographic quantum system. The entanglement structure of a genuine holographic quantum system is expected to be much more complex. The key point is that the study of these coarse-grained states will lead us to discover some properties of the entanglement structure in holographic quantum systems. In particular, in this paper, we will systematically demonstrate how the study of these coarse-grained states will lead to the necessity of perfect tensor entanglement in holographic quantum systems, with our preliminary work available in [63]. This section will demonstrate this in two aspects, where Sec. III A is a restatement of the conclusions of [63], while Sec. III B is entirely new. In Sec. IV, we will support our argument by constructing a more interesting locking thread configuration.

A. Characterizing entanglement entropy of disconnected regions

Characterizing the holographic entanglement entropy of disconnected regions using the coarse-grained state is nontrivial. Without loss of generality, let us focus on the entanglement entropy S_R of a nonconnected region $R = A_1 \cup A_3$ in Fig. 2. Suppose we already have a coarse-grained state $|\Psi\rangle_{\text{coarse}}$ corresponding to the top left of Fig. 2, which can characterize the entanglement entropies of all connected regions, i.e., $\{A_1, A_2, A_3, A_4, A_1 \cup A_2, A_2 \cup A_3\}$. We can further refine this coarse-grained state to obtain a new coarse-grained state $|\Psi'\rangle_{\text{coarse}}$, such that the new

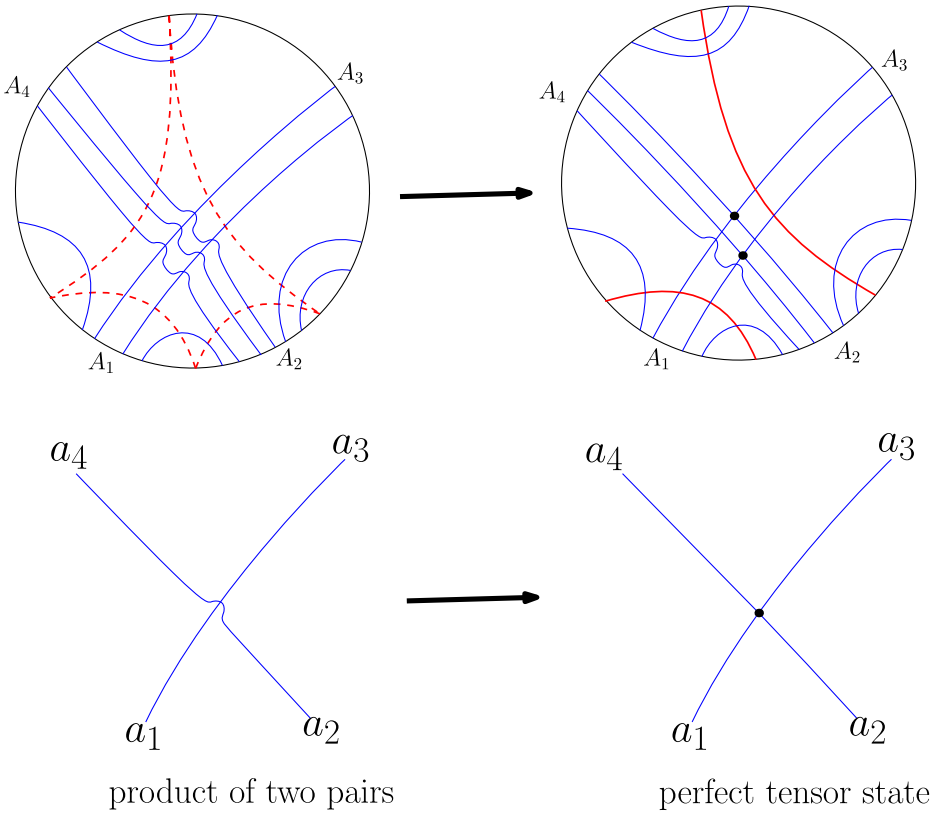

FIG. 2. The thread configuration in the upper left corresponds to a coarse-grained state constructed from the direct product of all pairwise entangled states, from which the entanglement entropies of all the connected subregions involved can be calculated. The top-right figure shows that in order for the original coarse-grained state to further characterize the entanglement entropy of an disconnected region $A_1 \cup A_3$, perfect entanglement must be introduced. The key point is illustrated at the bottom. Consider a thread connecting a site a_1 in A_1 and a site a_3 in A_3, and couple it to a thread connecting a site a_2 in A_2 and a site a_4 in A_4, so that the overall state of four qudits changes from (10) to (11).

coarse-grained state $|\Psi'\rangle_{\text{coarse}}$ can also characterize the entanglement entropy of the disconnected region R.

A simple method is pointed out in [63]. Note that, in the original thread configuration (see the top left of Fig. 2), intersecting threads do not influence each other. For example, consider two intersecting threads a_1a_3 and a_2a_4, apply the thread-state correspondence, and take $d = 3$. Then the overall state of the intersecting threads is simply the direct product of two pair-entangled states, i.e.,

$$|a_1a_2a_3a_4\rangle = \frac{1}{\sqrt{3}}(|0_{a_1}0_{a_3}\rangle + |1_{a_1}1_{a_3}\rangle + |2_{a_1}2_{a_3}\rangle) \otimes \frac{1}{\sqrt{3}}(|0_{a_2}0_{a_4}\rangle + |1_{a_2}1_{a_4}\rangle + |2_{a_2}2_{a_4}\rangle). \quad (10)$$

Now, the idea is to entangle these two noninteracting threads, making the overall state of the four qutrits a_1, a_3, a_2, a_4 a specific entangled state as follows:

$$|a_1a_2a_3a_4\rangle = \frac{1}{3}(|0_{a_1}0_{a_3}0_{a_2}0_{a_4}\rangle + |1_{a_1}1_{a_3}1_{a_2}0_{a_4}\rangle + |2_{a_1}2_{a_3}2_{a_2}0_{a_4}\rangle + |0_{a_1}1_{a_3}2_{a_2}1_{a_4}\rangle + |1_{a_1}2_{a_3}0_{a_2}1_{a_4}\rangle + |2_{a_1}0_{a_3}1_{a_2}1_{a_4}\rangle + |0_{a_1}2_{a_3}1_{a_2}2_{a_4}\rangle + |1_{a_1}0_{a_3}2_{a_2}2_{a_4}\rangle + |2_{a_1}1_{a_3}0_{a_2}2_{a_4}\rangle). \quad (11)$$

The key is that the original state (10) is not symmetric about the four qutrits. Note that in it, the entanglement entropy between qutrits $a_1 \cup a_2$ with $a_3 \cup a_4$ is $2\log 3$, while the entanglement entropy between qutrits $a_1 \cup a_2$ with $a_2 \cup a_4$ is 0. The reason is simple because a_1 and a_3 are at the two ends of the same thread, and a_2 and a_4 are at the two ends of the same thread. And these two threads are direct product. On the other hand, the new state is symmetric about the four qutrits. The state (11) is commonly referred to as a perfect tensor state in the literature. It can be more compactly written as (we adopt Einstein's index summation convention and omit the summation symbol)

$$|\chi\rangle = T_{\alpha\beta\mu\nu}|\alpha\beta\mu\nu\rangle, \tag{12}$$

where $|\alpha\beta\mu\nu\rangle = |\alpha\rangle \otimes |\beta\rangle \otimes |\mu\rangle \otimes |\nu\rangle$, and

$$T_{0000} = T_{1110} = T_{2220} = T_{0121} = T_{1201} = T_{2011} = T_{0212} = T_{1022} = T_{2102} = \frac{1}{3}, \tag{13}$$

while other components are 0. $T_{\alpha\beta\mu\nu}$ is an example of a (rank four) perfect tensor, and correspondingly, $|\chi\rangle$ is a perfect tensor state. The two "knotted" threads in the bottom right of Fig. 2 form a vertex extending four legs, essentially the graphical representation of $T_{\alpha\beta\mu\nu}$ in tensor network language. The key is to realize that this state has an interesting property: for any one of the four qutrits, the entanglement entropy between it and its complement is $\log 3$, and for any two of them with their complement, the entanglement entropy is $2\log 3$. Perfect tensor states are well-known ingredients in the holographic HaPPY code used for quantum error correction [12] and are also known as absolutely maximally entangled states in quantum information theory [102,103]. More generally, perfect tensors can be defined equivalently in two ways:

Definition 1. A $2s$-perfect tensor is a $2s$-qudit pure state for any positive integer s such that the reduced density matrix involving any s qudits is maximally mixed.

Definition 2. A $2s$-perfect tensor is a $2s$-qudit pure state for any positive integer $k \leq s$ such that the mapping from the states of any k qudits to the states of the remaining $2s - k$ qudits is an isometric isomorphism.

In summary, by replacing the tensor product states with perfect tensor states, it is possible to characterize the entanglement entropy of disconnected regions using coarse-grained states. More detailed discussions can be found in [63]. We will further indicate in Sec. V A that perfect tensor entanglement is inevitable for characterizing the entanglement entropies of disconnected regions.

B. Characterizing the entanglement wedge cross section

In this subsection, we point out another noteworthy phenomenon that once again indicates the inevitability of perfect tensor entanglement for the entanglement structure of holographic quantum systems at the coarse-grained level. This phenomenon is related to the holographic entanglement wedge cross section.

Taking Fig. 3(a) as an example, let us consider the correlation between two adjacent subregions A_1 and A_2 in the conformal field theory (CFT). Within the framework of holographic principles, this quantity can be measured by the area of a so-called entanglement wedge cross section $\sigma_{A_1:A_2}$ [97,98]. The definition of the entanglement wedge cross section $\sigma_{A_1:A_2}$ is as follows: first, define the entanglement wedge $W(A)$ of $A = A_1 \cup A_2$ as the bulk region enclosed by A and its corresponding RT surface γ_A. Then, a minimal extremal surface $\sigma_{A_1:A_2}$ can be defined, satisfying: (1) it divides the entanglement wedge $W(A)$ into two parts, one entirely touching A_1 and the other entirely touching A_2; (2) among all extremal surfaces satisfying condition 1, select the one with the smallest area.

Now, there is a holographic method to calculate the area of this surface [99]. As shown in Fig. 3(b), first, we find a point Q_* on the complement B of A to divide B into two parts B_1 and B_2. Consequently, we can construct a locking

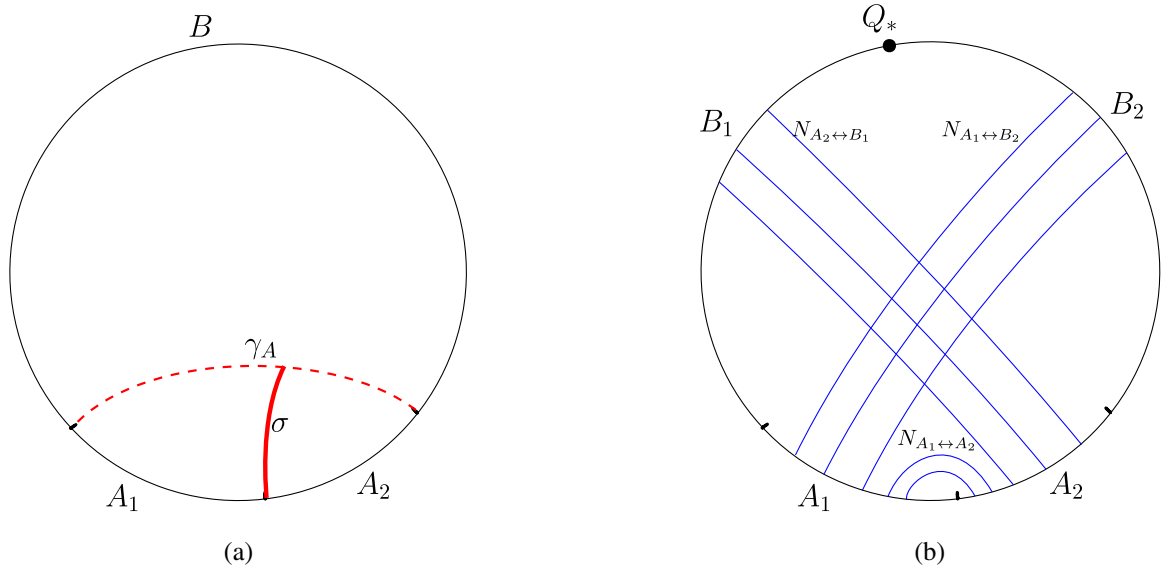

FIG. 3. (a) The correlation between two adjacent subregions A_1 and A_2 can be holographically measured by the area of the entanglement wedge cross section $\sigma_{A_1:A_2}$, represented by the red solid line. (b) The BPE method to calculate the area of $\sigma_{A_1:A_2}$: divide the complement B into two parts such that $N_{A_1\leftrightarrow B_2} = N_{A_2\leftrightarrow B_1}$.

thread configuration corresponding to the basic region selection $\{A_1, A_2, B_1, B_2\}$ to characterize the entanglement structure at this coarse-grained level. The requirement is to find a point Q_* such that, in its corresponding thread configuration, the number of threads connecting A_1 and B_2 is equal to the number of threads connecting A_2 and B_1,

$$N_{A_1\leftrightarrow B_2} = N_{A_2\leftrightarrow B_1}. \tag{14}$$

Then, we can obtain

$$\frac{\mathrm{Area}(\sigma_{A_1:A_2})}{4G_N} = N_{A_1\leftrightarrow B_2} + N_{A_1\leftrightarrow A_2}. \tag{15}$$

This interesting fact was first proposed in the language of partial entanglement entropy in the paper [99] and is known as the balanced partial entropy method. The right-hand side of (15) is named as BPE.

So, how do we understand this method of probing the geometric area? Essentially, the area of the surface $\sigma_{A_1:A_2}$ measures the correlation between the two parts A_1 and A_2 in A.[5] When we apply the concept of coarse-grained states of thread configurations to understand this "experimental fact," we will once again see the necessity of perfect tensor states.

The key point remains that we must "entangle" the threads connecting A_1 and B_2 with the threads connecting A_2 to B_2 to form a perfect tensor state (11) about the four qutrits. As shown in Fig. 3(b), once we handle the coarse-grained state in this way, it becomes clear that the correlation between A_1 and A_2 is precisely composed of two parts. One part [the second term in (15)] is contributed by the bipartite entanglement

$$|a_1a_2\rangle = \frac{1}{\sqrt{3}}(|0_{a_1}0_{a_2}\rangle + |1_{a_1}1_{a_2}\rangle + |2_{a_1}2_{a_2}\rangle), \tag{16}$$

where between a_1 and a_2 there exists $\log 3$ of entanglement. The other part [the first term in (15)] is contributed by the perfect tensor entanglement

$$\begin{aligned}|a_1b_2a_2b_1\rangle = \frac{1}{3}(&|0_{a_1}0_{b_2}0_{a_2}0_{b_1}\rangle + |1_{a_1}1_{b_2}1_{a_2}0_{b_1}\rangle \\ &+ |2_{a_1}2_{b_2}2_{a_2}0_{b_1}\rangle + |0_{a_1}1_{b_2}2_{a_2}1_{b_1}\rangle \\ &+ |1_{a_1}2_{b_2}0_{a_2}1_{b_1}\rangle + |2_{a_1}0_{b_2}1_{a_2}1_{b_1}\rangle \\ &+ |0_{a_1}2_{b_2}1_{a_2}2_{b_1}\rangle + |1_{a_1}0_{b_2}2_{a_2}2_{b_1}\rangle \\ &+ |2_{a_1}1_{b_2}0_{a_2}2_{b_1}\rangle),\end{aligned} \tag{17}$$

[5]In previous studies, this correlation has been understood as various quantum information theory quantities such as EoP [97,98], BPE [99–101], reflected entropy [104], logarithmic negativity [105,106], odd entropy [107], differential purification [108], etc.

where a_1 is symmetrically entangled with the other three qutrits in its complement, which introduces $\log 3$ of correlation between a_1 and a_2.

Once again, we see the necessity of perfect state entanglement. Because if we only use bipartite entanglement, that is, if we do not entangle the threads connecting A_1 and B_2 with the threads connecting A_2 to B_2, there will be no correlation between a_1 and a_2 at this point, as seen in its corresponding expression,

$$\begin{aligned}|a_1b_2a_2b_1\rangle = &\frac{1}{\sqrt{3}}(|0_{a_1}0_{b_2}\rangle + |1_{a_1}1_{b_2}\rangle + |2_{a_1}2_{b_2}\rangle) \\ &\otimes \frac{1}{\sqrt{3}}(|0_{a_2}0_{b_1}\rangle + |1_{a_2}1_{b_1}\rangle + |2_{a_2}2_{b_1}\rangle),\end{aligned} \tag{18}$$

because at this point, the two threads a_1b_2 and a_2b_1 are independent of each other. In this way, we would miss the first contribution in (15) and fall into contradiction.

In this paper, we will only consider the case where A_1 and A_2 are adjacent. Similar results, as in (15), will still appear for the case where A_1 and A_2 are not adjacent. However, the physical analysis is entirely similar.

IV. A MORE CONCRETE MODEL: THREAD CONFIGURATIONS WITH MERA STRUCTURE

In this section, we will construct a more nontrivial thread configuration to further elucidate our proposal introduced in the previous section, namely, the necessity of perfect tensor entanglement for holographic quantum systems at the coarse-grained level. Specifically, we construct a thread configuration with a MERA structure [7–11]. MERA structure originated as a tensor network method invented for characterizing the ground state of critical systems that do not satisfy the area law [7–9]. It has been considered in [10,11,37] to simulate a time slice of anti–de Sitter (AdS) spacetime in the holographic duality and was later proposed to be closely related to the kinematic space corresponding to AdS space in [41,87]. Therefore, it is a highly important and insightful structure in the research of holographic duality.

Our approach is as follows: first, we will show that the MERA tensor network automatically generates a locking thread configuration. In other words, we construct a specific thread configuration with a MERA structure. This allows us to study its corresponding coarse-grained state. Consequently, we can further introduce perfect tensor entanglement to this coarse-grained state and demonstrate how this procedure resolves issues encountered in characterizing the holographic entanglement entropies of disconnected regions and the correlations dual to entanglement wedge cross sections.

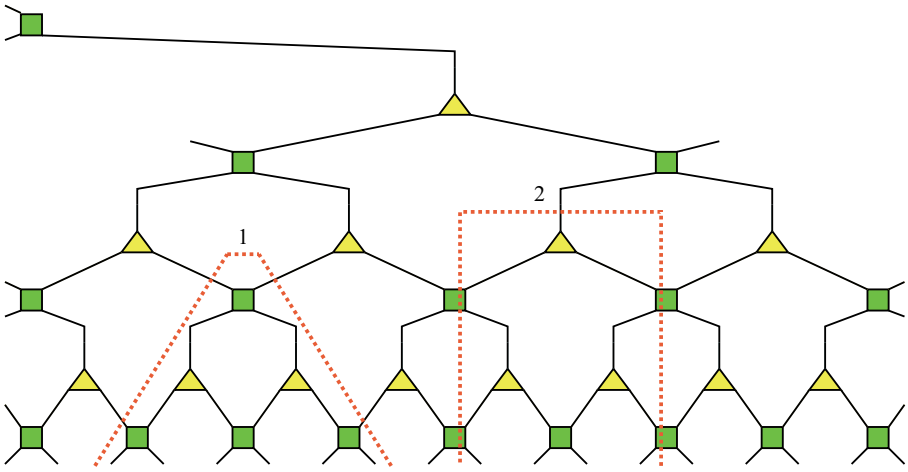

FIG. 4. The MERA tensor network, composed of two basic tensors. The coarse grainers are represented by three-leg triangles, the disentanglers are represented by four-leg squares. The red dashed lines 1 and 2 represent two choices of defining an RT surface.

A. MERA tensor network naturally generates a thread configuration

As shown in Fig. 4, the MERA tensor network is composed of two basic tensors [7–9]. The first type of tensor is called the coarse grainer w, which is an isometry, satisfying

$$w^\dagger w = 1. \tag{19}$$

It is generally represented by a triangle in the diagram and has three legs, indicating that it represents a rank-three tensor. The other type of tensor is called the disentangler u, which is a unitary operator, satisfying

$$u^\dagger u = 1, \qquad uu^\dagger = 1. \tag{20}$$

It is typically represented by a square in the diagram and has four legs, indicating that it represents a rank-four tensor. MERA is a hierarchical array, representing entanglement at different length scales through alternating layers of coarse grainers and disentanglers. As the coarse-graining process proceeds, the disentangling layer is responsible for reducing the quantum entanglement of the ground state, which was highly entangled originally. Generally, when the wave function can be written as a direct-product state (an unentangled state), the network terminates. However, for cases with scale invariance, the tensor network has infinite depth. It must be noted that the MERA tensor network is, in fact, a general method for constructing arbitrary quantum states (not limited to critical quantum systems), and its construction recipe depends on the specific form given to the isometry w and the disentangler u.

Swingle [10,11] first proposed that a MERA tensor network can simulate a discretization of a time slice of AdS spacetime, particularly, it can characterize the discretized RT formula. In Fig. 4, we illustrate the concept of the RT surface in the network. It is a "cut" that divides the entire network into two parts, satisfying: (1) one part only touches A, and the other part only touches B, the complement of A; (2) among all cuts satisfying condition 1, select the one with the minimum number of cut legs. In the MERA tensor network, it can be argued that the number of legs the cut passes through exactly gives the entanglement entropy of region A (more precisely, an upper bound on the entanglement entropy). Thus, by defining the number of legs the cut passes through as the area of the cut, we return to the RT formula.

Although not necessarily related to our main theme, let us point out one intuitive motivation from the perspective of bit-thread representation that leads to the generation of a thread configuration by the MERA tensor network. In the bit-thread representation, a Planck area is usually allowed to accommodate the passage of one bit thread [53–56]. In other words, the number of bit threads is proportional to the area measure of the channel cross section. Now, since in the MERA tensor network, the number of legs cut by the RT cut plays the role of the area measure, we can naturally regard each leg as a channel carrying a network flow. We agree that the number of threads passing through this channel is precisely equal to the logarithm of the dimension of the leg. The practical implementation of this idea is shown in Fig. 5(a). Note that we do not require a general construction; in fact, we choose very simple (even trivial in their own right) representations of disentanglers and coarse grainers, and such choices should not be expected to capture the ground state of a true CFT. However, our goal is to construct a coarse-grained state, and what we want to retain is the skeletal structure of MERA itself.[6]

[6]It was actually proposed in [37] that the skeletal structure of the MERA tensor network plays a role in gluing spacetime fragments, which themselves are represented by the so-called Euclidean tensors, into an AdS time slice.

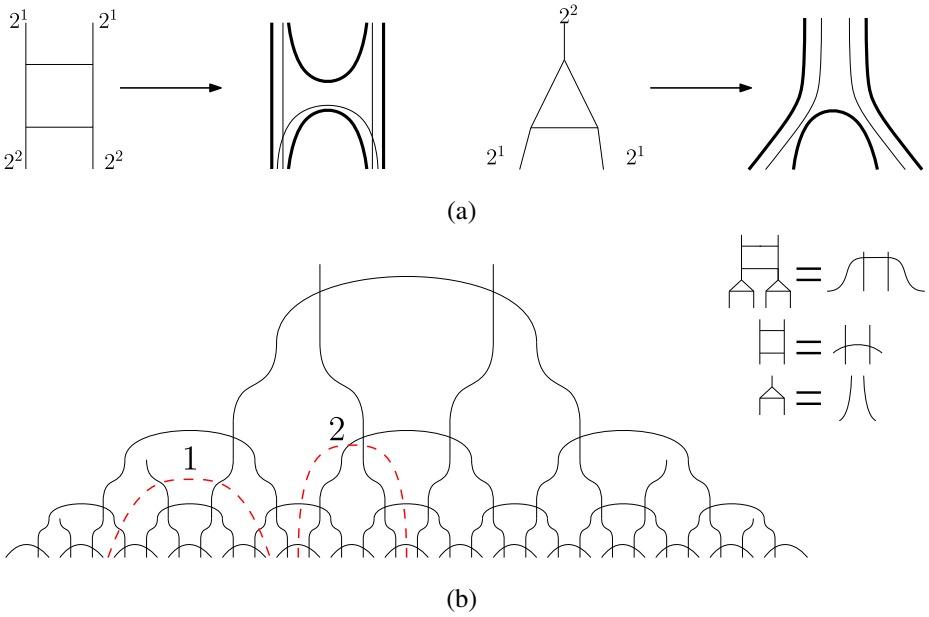

FIG. 5. Regarding the legs of each fundamental tensor as channels carrying thread flows will generate an overall thread configuration. The red dashed lines in (b) represent the RT surfaces in this context. Note that in (a) we choose very simple thread representations of disentanglers and coarse grainers.

Regarding each fundamental tensor as corresponding to channels carrying a subset of thread flows immediately generates an overall thread configuration, as shown in Fig. 5(a). This configuration can be understood as being composed of many small thread configurations glued together according to the MERA structure. The first thing we can immediately check about this overall thread configuration is that it automatically satisfies the locking property of the thread configurations reviewed in Sec. II A. That is, we can directly and precisely calculate the entanglement entropy of a specified connected boundary subregion from this thread configuration. Specifically, consider a boundary subregion A of this thread configuration, which consists of end points of a set of threads. Now, if we examine the RT surface γ_A corresponding to A in the MERA tensor network, we find that the RT surface exactly divides this thread configuration into two halves, such that each thread passes through γ_A at most once, and the number of threads passing through γ_A exactly gives the entanglement entropy of A (or precisely the area of γ_A). Clearly, the red thread 1 marked in the figure as the RT surface is consistent with the interpretation in the thread configuration viewpoint. We can also define the area of the RT surface by counting the number of cut disentanglers [109], as shown by the red thread 2, which cuts the "inner threads" of the disentanglers. Nevertheless, cutting the legs of the MERA tensor network can then be interpreted in our construction as cutting the number of threads connecting the interior of region A and the remaining part, and the number of these threads gives the entanglement entropy of A, very similar to the picture proposed in the bit-thread representation. Early discussions on the connection between bit threads and MERA tensor networks can be found in [71].

Let us point out that if, as shown in Fig. 6(a), we choose another way to construct disentanglers and coarse grainers, we can also obtain a thread configuration. Moreover, if we examine the trajectory of the RT surface, the above considerations still hold, meaning that we still get a locking thread configuration. In fact, the structures of these two configurations are essentially the same, except for a small difference in the first layer. They are topologically identical and can be equivalently characterized by the diagram in Fig. 6(b). This is because, as shown in Fig. 6(a), taking two coarse grainers connected by one disentangler in the previous layer as a basic unit, the local thread configurations obtained by the two construction methods are the same. For symmetry considerations in the diagram, we uniformly define the RT surface as shown in the figure, presenting a shape similar to a light cone. Note that, for our current purposes, this diagram has only topological significance; however, we present it as a regular pattern, which, in appearance, is arranged in alternating tiles of quadrilaterals and pentagons. Still, keep in mind that, in the current context, these threads only overlap with each other and are not "coupled" together (we will discuss the significance of coupling later). This regular pattern facilitates our understanding of the precise correspondence between the MERA structure and kinematic space.

Why do we not choose a thread configuration representation of basic tensors as shown in Fig. 7? This is because, in this representation, long-range entanglement

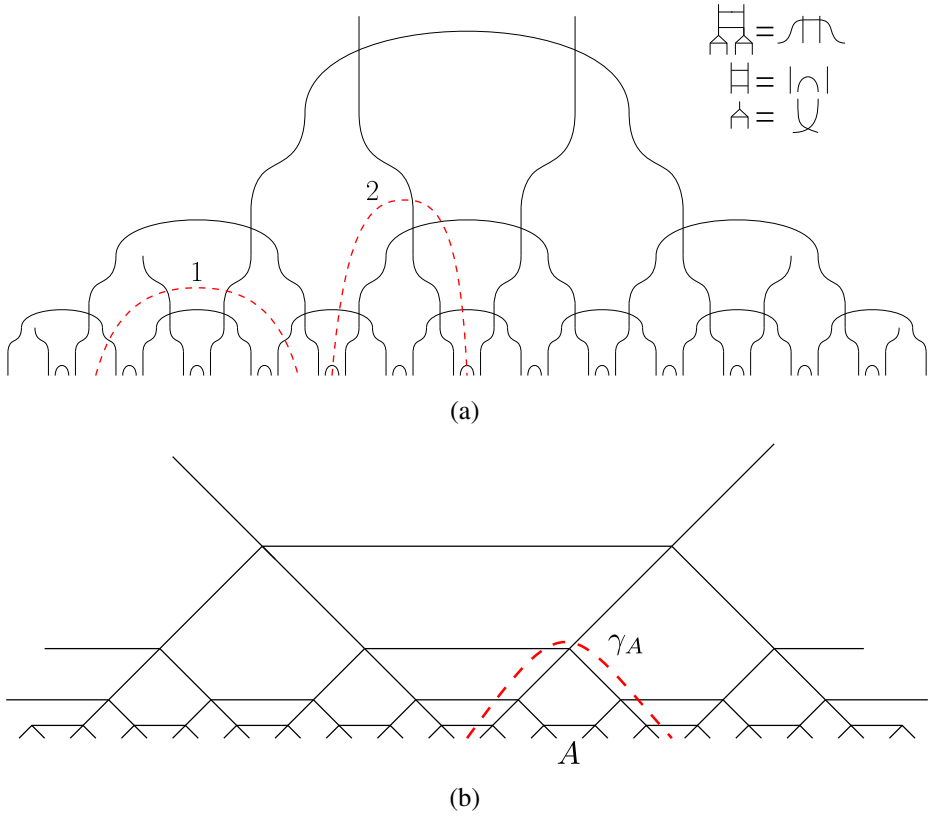

FIG. 6. (a) Another thread construction of disentanglers and coarse grainers lead to a similar thread configuration. (b) Another representation of the thread configuration with a MERA structure, which has the same topology.

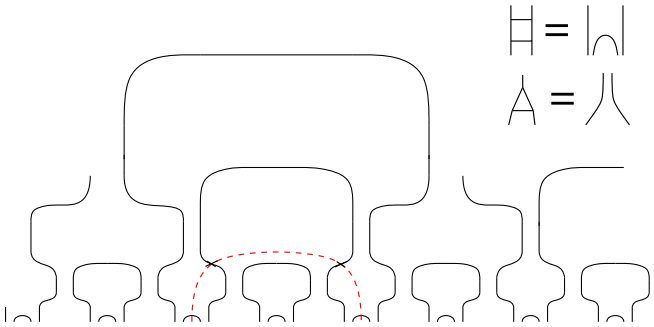

FIG. 7. An illegal thread construction for our purposes.

cannot be conveniently characterized, as shown in Fig. 7. Moreover, the application of the RT formula may also encounter difficulties because the RT surface defined by the minimum cut may pass through the same thread twice. In other words, the MERA state constructed in this way, with the minimum cut, only characterizes the upper bound of the entanglement entropy of the corresponding region and is not exactly equal. Therefore, we choose to construct the thread configuration that satisfies our motivation. In fact, we realize that there are multiple constructions of thread configurations that meet our requirements. For example, as long as we arrange the dimensions of bonds of disentanglers and coarse grainers appropriately, we can construct more general thread configuration states. However, we only want to discuss what interesting properties the MERA structure will bring to the thread configuration, so we choose the simplest case.

B. Coarse-grained state corresponding to the thread configuration

Now let us provide a more physical interpretation for the above intuition. In fact, Fig. 8(a) perfectly conforms to the rules of the thread-state correspondence reviewed in Sec. II B. More specifically, each thread can be considered to correspond to a Bell state,

$$|\text{red}\rangle = |0_1 0_2 \cdots 0_n\rangle,$$
$$|\text{blue}\rangle = |1_1 1_2 \cdots 1_n\rangle. \tag{21}$$

In this context, that a thread is said to pass through multiple qudits is because, as constructed in Fig. 8(a), a global thread actually results from gluing together the legs of different positions of disentanglers and coarse grainers. As a result, by focusing on the thread things, we are visualizing the entanglement between different fundamental tensors.

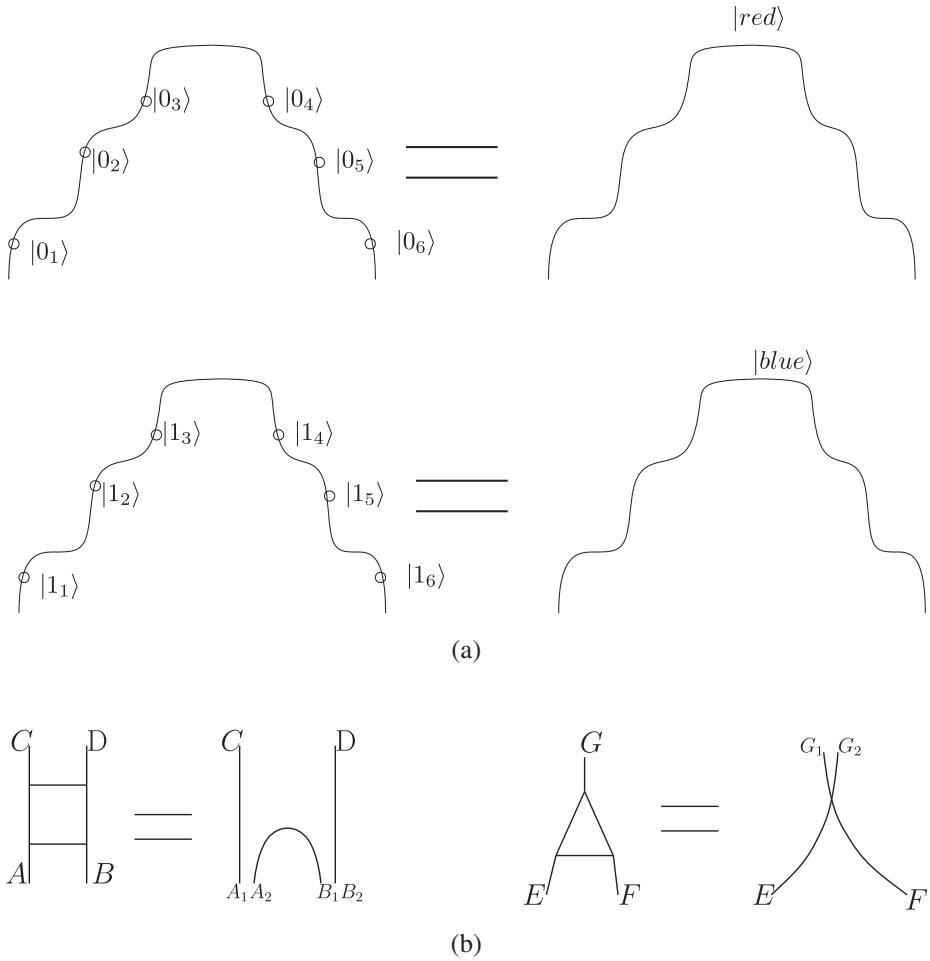

FIG. 8. (a) A global thread defined from gluing together the legs of different basic tensors conforms to the rules of the thread-state correspondence. (b) Essentially, we construct the basic tensors as the coarse-grained states of local thread configurations.

To explicitly show that the thread configurations with MERA structure we constructed can be included in the framework of the thread-state interpretation [61–63], we provide a physical interpretation for the thread representation of disentanglers and coarse grainers as shown in Fig. 8(b). Essentially, we construct a special disentangler tensor by using local thread configurations, where each local thread segment represents a Bell pair, and the resulting disentangler is simply the tensor product of these Bell states, i.e.,

$$\begin{aligned}|u_{A_1A_2B_1B_2CD}\rangle = &\frac{1}{\sqrt{2}}(|0_{A_1}0_C\rangle + |1_{A_1}1_C\rangle)\\ &\otimes\frac{1}{\sqrt{2}}(|0_{B_2}0_D\rangle + |1_{B_2}1_D\rangle)\\ &\otimes\frac{1}{\sqrt{2}}(|0_{A_2}0_{B_1}\rangle + |1_{A_2}1_{B_1}\rangle).\end{aligned} \tag{22}$$

To show that this satisfies the unitary condition (20), we redefine

$$\begin{aligned}|0'0'\rangle_{AB} &= |0_{A_1}0_{B_2}\rangle\otimes\frac{1}{\sqrt{2}}(|0_{A_2}0_{B_1}\rangle + |1_{A_2}1_{B_1}\rangle),\\ |0'1'\rangle_{AB} &= |0_{A_1}1_{B_2}\rangle\otimes\frac{1}{\sqrt{2}}(|0_{A_2}0_{B_1}\rangle + |1_{A_2}1_{B_1}\rangle),\\ |1'0'\rangle_{AB} &= |1_{A_1}0_{B_2}\rangle\otimes\frac{1}{\sqrt{2}}(|0_{A_2}0_{B_1}\rangle + |1_{A_2}1_{B_1}\rangle),\\ |1'1'\rangle_{AB} &= |1_{A_1}1_{B_2}\rangle\otimes\frac{1}{\sqrt{2}}(|0_{A_2}0_{B_1}\rangle + |1_{A_2}1_{B_1}\rangle).\end{aligned} \tag{23}$$

With this, the disentangler tensor can be expressed as u_{ABCD}, and it satisfies

$$u_{0'0'00} = u_{0'1'01} = u_{1'0'10} = u_{1'1'11} = \frac{1}{2}, \tag{24}$$

which indeed conforms to the condition (20) and thus is a unitary tensor. Similarly, it is not difficult to verify that the coarse-graining tensor in Fig. 8(b) is an isometry. Likewise, it is a tensor product of three Bell states, where

$$|w_{EFG_1G_2}\rangle = \frac{1}{\sqrt{2}}(|0_E 0_{G_2}\rangle + |1_E 1_{G_2}\rangle) \otimes \frac{1}{\sqrt{2}}(|0_F 0_{G_1}\rangle + |1_F 1_{G_1}\rangle). \quad (25)$$

Define

$$\begin{aligned} |0'\rangle_G &= |0_{G_2}\rangle \otimes |0_{G_1}\rangle, \\ |1'\rangle_G &= |0_{G_2}\rangle \otimes |1_{G_1}\rangle, \\ |2'\rangle_G &= |1_{G_2}\rangle \otimes |0_{G_1}\rangle, \\ |3'\rangle_G &= |1_{G_2}\rangle \otimes |1_{G_1}\rangle. \end{aligned} \quad (26)$$

With this, the coarse grainer can be written as w_{EFG}, and it satisfies

$$w_{000'} = w_{011'} = w_{102'} = w_{113'} = \frac{1}{2}, \quad (27)$$

which indeed satisfies condition (19). The same method can also be used to explain the state interpretation corresponding to the construction method in Fig. 6(a).

Now, we focus our attention on the thread-state representations (22) and (25) of the fundamental tensors u and w. It can be seen that, when connecting (contracting) fundamental tensors at different positions, the global thread only needs to exhibit two overall states $|\text{red}\rangle$ and $|\text{blue}\rangle$, as each local thread segment representing a Bell pair essentially provides a unitary mapping between two sites. A global thread vividly represents the transmission path of information.

C. Connection with kinematic space

We have demonstrated that the constructed thread configuration with MERA structure is precisely a locking thread configuration in the sense of Sec. II. As a result, this thread configuration can be used to calculate the entanglement entropy between any connected subregion and its complement, which will precisely equal the number of connecting threads. Moreover, by employing the thread-state correspondence, one can partially trace over the coarse-grained states corresponding to this thread configuration to prove this result. Additionally, in this framework, the number of threads connecting two regions A_i and A_j precisely gives half the value of the conditional mutual information $I(A_i, A_j|L)$, where L represents the region between A_i and A_j.

Now, it is interesting to compare the thread configuration with MERA structure with kinematic space [41,87].[7] For AdS_3, kinematic space is a two-dimensional dual space. The points in this space, denoted in light-cone coordinates as (u, v), are obtained by mapping each pair of points parametrized by coordinates u, v on the one-dimensional time slice of the original CFT_2. The essential feature of kinematic space is that its metric (or spatial volume density) is defined by the conditional mutual information. In other words, $\frac{1}{2}I(A_i, A_j|L)$ is precisely given by the volume of a diamond-shaped region $\diamond_{A_i,A_j|L}$, defined as the region enclosed by the light rays starting from the end points of A_i and A_j at the boundary of kinematic space,

$$\frac{1}{2}I(A_i, A_j|L) = \text{vol}(\diamond_{A_i,A_j|L}). \quad (28)$$

In [41,87], the MERA tensor network is identified as a kinematic space itself, and the conditional mutual information $\frac{1}{2}I(A_i, A_j|L)$ is interpreted as the number of isometries inside the counterpart of $\diamond_{A_i,A_j|L}$ in MERA. Let us carefully examine this viewpoint. In our framework, the volume measure of the kinematic space, represented by the conditional mutual information, is explicitly given by the number of disentangler tensors in MERA. This quantity is also related to the so-called entanglement density in [109]. The reason is intuitive: as illustrated in Fig. 9(a), considering the RT surfaces γ_{A_i} and γ_{A_j} corresponding to two connected subregions A_i and A_j, respectively, $\frac{1}{2}I(A_i, A_j|L)$ represents the number of threads simultaneously crossing γ_{A_i} and γ_{A_j}. However, note that now the number of these threads precisely matches the number of "horizontal lines" inside the counterpart of diamond-shaped region $\diamond_{A_i,A_j|L}$ in our thread configuration. Reviewing the thread representation of disentanglers in Fig. 5(a), each horizontal line actually corresponds to a disentangler tensor. Therefore, in our framework, $\frac{1}{2}I(A_i, A_j|L)$ precisely corresponds to the number of disentangler tensors inside the diamond-shaped region $\diamond_{A_i,A_j|L}$. The discussion of the connection between entanglement density and conditional mutual information has also been explored in [64]. It is worth noting that, in [41,87], the conditional mutual information is argued to be given by the number of isometries (i.e., the coarse grainers). Since in the MERA tensor network isometries and disentanglers are added successively, the number of both along the light-cone direction is consistent.

Note that, in the general MERA construction, one can only argue that the upper limit of the entanglement entropy of a subregion A is given by the minimum number of cuts. In the model we constructed, however, the entanglement entropy is designed to be strictly saturated, i.e., $S(A)$ is exactly proportional to the minimum number of cuts. Thus, our model helps demonstrate the structural mechanism of the connection between MERA and the nature of kinematic space. Moreover, the equivalence of conditional mutual information and the number of disentangler tensors in our model is exact [109]. Another thing to note is that, as we

[7]The connection between kinematic space and bit threads is also discussed in [64].

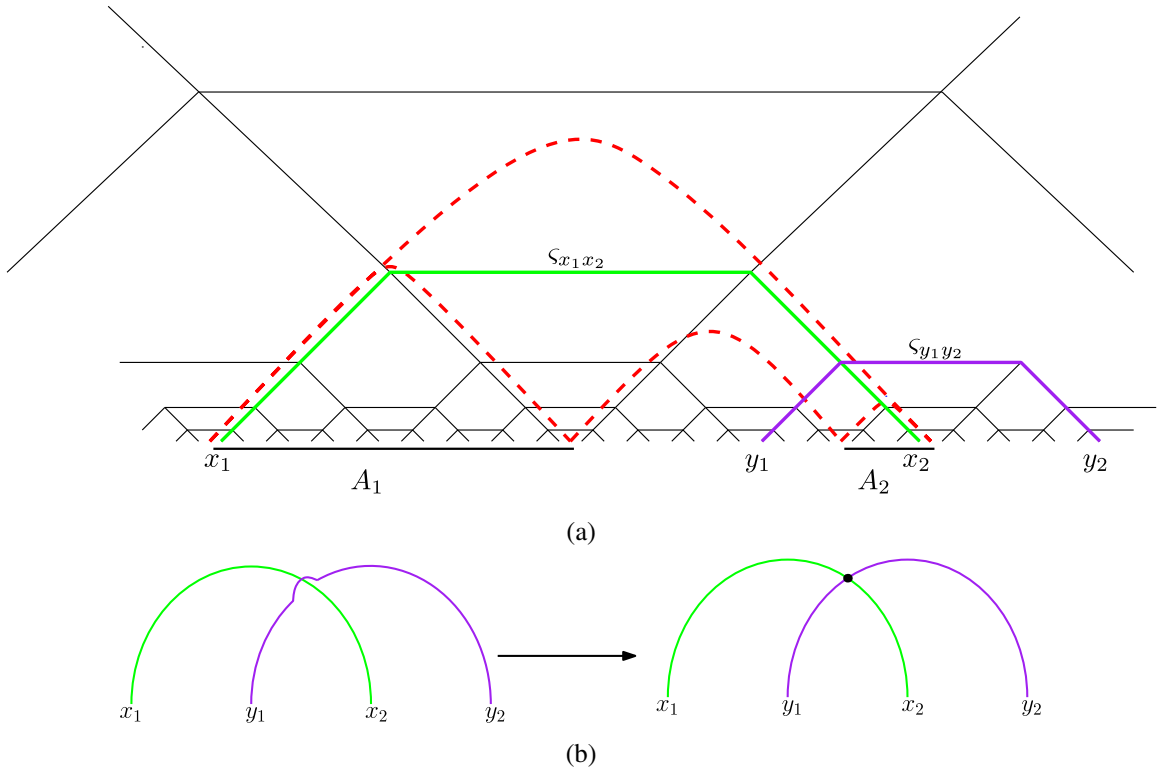

FIG. 9. (a) For two nonadjacent subregions (separated by L), the green lines here represent the internal entanglement. The number of these internal threads matches the number of disentanglers inside the region $\diamondsuit_{A_i,A_j|L}$ in kinematic space. Furthermore, to characterize the entropy of the union of the two, the green lines should entangle with the purple lines, which represent the entanglement within the complement. Red dashed lines represent RT surfaces. (b) Entangle the threads such that there is 2 log 2 of entanglement between $x_1 \cup x_2$ and $y_1 \cup y_2$.

have consistently emphasized, what we constructed is not a MERA state that truly characterizes the ground state of a CFT, but rather a coarse-grained state. However, such a MERA state is sufficient to characterize the properties that kinematic space portrays. In a sense, kinematic space does not present many other important aspects of a truly ground-state MERA state characterizing a CFT, but rather reflects its skeletal structure.

V. CHARACTERIZATION OF ENTANGLEMENT ENTROPY FOR DISCONNECTED REGIONS

A. Perfect tensor states couple bipartite correlations

As reviewed in Sec. III A, a significant challenge of the coarse-grained state of this thread configuration is its inability to consistently characterize the entanglement entropies of disconnected regions. This paradox is explicitly pointed out in [63]. Simply put, in the current scenario, consider a disconnected region A shown in Fig. 9(a), composed of two nonadjacent parts A_1 and A_2, i.e., $A = A_1 \cup A_2$. The goal is to compute its entanglement entropy. Assuming the sizes of A_1 and A_2 are relative small compared to the size of their separation, according to the RT formula, then the RT surface should be $\Gamma = \gamma_1 \cup \gamma_2$, where γ_1 and γ_2 are the RT surfaces corresponding to A_1 and A_2, respectively. However, interpreting the quantum state of thread configurations as a direct product of threads equipped with Bell states cannot correctly provide a self-consistent account of the entanglement entropy for $A = A_1 \cup A_2$. As shown in the figure, the reason is that, when the same thread (e.g., the thread connecting the point x_1 inside A_1 and the point x_2 inside A_2, denoted as $\varsigma_{x_1x_2}$) simultaneously passes through the surfaces γ_1 and γ_2, the entanglement represented by this thread should be regarded as the internal entanglement of A, thus not contributing to the entanglement entropy of A. More explicitly, calculations based on the direct-product coarse-grained state correctly provides the entanglement entropy for A_1 and A_2 themselves, but the resulting entanglement entropy for A calculated by the same direct-product coarse-grained state will be less than the expected $S(A) = S(A_1) + S(A_2)$; the difference is precisely proportional to the number of threads simultaneously passing through γ_1 and γ_2, or in other words, the number of threads connecting A_1 and A_2, i.e., half of the conditional mutual information between A_1 and A_2.

This implies the necessity to design entanglement beyond bipartite. The reason can be seen from a simple

analysis. As shown in Fig. 9(a), let us imagine another thread $\varsigma_{y_1y_2}$ connecting points y_1 and y_2 outside region A. $\varsigma_{y_1y_2}$ and $\varsigma_{x_1x_2}$ are superficially overlapping. Asking for the entanglement entropy between $x_1 \cup x_2$ and $y_1 \cup y_2$, we first write down the state of $x_1 \cup x_2 \cup y_1 \cup y_2$ as a whole. According to the thread-state rules, if we assume that there is no entanglement between the two threads $\varsigma_{y_1y_2}$ and $\varsigma_{x_1x_2}$, then

$$|x_1x_2y_1y_2\rangle = \frac{1}{\sqrt{2}}(|0_{x_1}0_{x_2}\rangle + |1_{x_1}1_{x_2}\rangle) \otimes \frac{1}{\sqrt{2}}(|0_{y_1}0_{y_2}\rangle + |1_{y_1}1_{y_2}\rangle). \quad (29)$$

Obviously, the entanglement entropy between $x_1 \cup x_2$ and $y_1 \cup y_2$ is 0 in (29). The key is that (29) is not symmetric for the four indices x_1, x_2, y_1, y_2. If we consider the entanglement entropy between a single index and the other three indices, we get $\log 2$. However, if we consider the entanglement entropy between two specified indices and the other two, different situations arise. For example, considering the entanglement entropy between $x_1 \cup y_1$ and $x_2 \cup y_2$, we get $2\log 2$, while considering the case between $x_1 \cup x_2$ and $y_1 \cup y_2$ results in 0.

That the thread $\varsigma_{x_1x_2}$ represents the internal entanglement of $A = A_1 \cup A_2$ is equivalent to saying that $\varsigma_{x_1x_2}$ and $\varsigma_{y_1y_2}$ have no entanglement between them. To obtain the correct entanglement entropy $S(A)$ as the sum of the areas of γ_1 and γ_2, we should hope $x_1 \cup x_2$ as a whole to provide $2\log 2$ of entanglement with $y_1 \cup y_2$. Therefore, we should modify the state (29) to be completely symmetric for all four indices. As reviewed in Sec. III, perfect tensor states can satisfy this requirement. Let us recopy it as follows:

$$\begin{aligned}|x_1x_2y_1y_2\rangle = \frac{1}{3}(&|0_{x_1}0_{x_2}0_{y_1}0_{y_2}\rangle + |1_{x_1}1_{x_2}1_{y_1}0_{y_2}\rangle \\ &+ |2_{x_1}2_{x_2}2_{y_1}0_{y_2}\rangle + |0_{x_1}1_{x_2}2_{y_1}1_{y_2}\rangle \\ &+ |1_{x_1}2_{x_2}0_{y_1}1_{y_2}\rangle + |2_{x_1}0_{x_2}1_{y_1}1_{y_2}\rangle \\ &+ |0_{x_1}2_{x_2}1_{y_1}2_{y_2}\rangle + |1_{x_1}0_{x_2}2_{y_1}2_{y_2}\rangle \\ &+ |2_{x_1}1_{x_2}0_{y_1}2_{y_2}\rangle). \end{aligned} \quad (30)$$

More thoroughly, to address the issue of characterizing the entanglement entropies of disconnected regions, we can propose a natural picture: in the original thread configuration, although bulk threads may appear to "intersect" with each other, they are actually not coupled with each other. This means that the state of the thread configuration is simply the direct product of the quantum states corresponding to these threads. Now imaging the threads coupling with each other at all intersection points [see Fig. 9(b)], the original thread configuration becomes a tensor network composed of rank-four tensors. More explicitly, we assume that these rank-four tensors are recognized as perfect tensors. This is actually a concrete implementation of the idea proposed recently in [63].

A natural way to argue for this approach is to use recursive thinking: At the beginning, in the original "direct-product state" picture, we have already successfully characterized the entanglement entropies of all connected subregions. Then we can gradually couple one "internal thread" (such as $\varsigma_{x_1x_2}$) with one "external thread" (such as $\varsigma_{y_1y_2}$) for specified disconnected subregions (such as $A = A_1 \cup A_2$) to further characterize the entanglement entropies of the specified disconnected regions, without changing other entanglement structures. By adding entanglement into all threads at all "intersections" in this step-by-step way, it can be expected that the entanglement entropies of all disconnected regions can be consistently characterized. We will provide a more rigorous proof in the next section.

The issue of characterizing the entanglement entropies of disconnected regions also suggests that kinematic space cannot be simply related to a simple direct product of the quantum states of each spatial point, even though in kinematic space the entropy corresponding to the diamond-shaped region is notably proportional to its volume. This is because now the threads that are one-to-one mapped with the spatial points in kinematic space should be understood as being entangled with each other. Therefore, points in kinematic space are also highly entangled with each other.

B. Proof

First, we point out that assigning a rank-four perfect tensor state to each "four-legged subdiagram" in the "entangled thread configuration" and eventually unambiguously gluing these small tensors together is feasible. We agree to label each rank-four perfect tensor as $T_{\alpha\beta\mu\nu}$, where the order of the four qutrits α, β, μ, ν is important. In other words, once we specify the four legs of a four-legged subdiagram as being respectively associated with α, β, μ, ν, the entangled state of the four qutrits as a whole is defined according to the pattern specified in Eq. (12). Now, contraction implies index summation, so to avoid ambiguity, we stipulate that when two adjacent four-legged subdiagrams are glued, legs with the same label are always connected, as shown in Fig. 10. Thus, when dealing with an entire tensor network diagram glued together by multiple four-legged diagrams, the unambiguous requirements for tensor contraction are equivalent to the need to assign index types $\alpha, \beta, \mu,$ or ν to each leg in the tensor network, ensuring that legs sharing a vertex cannot be assigned the same index types. Fortunately, this is explicitly achievable. Considering each index type as a color and each leg in the network as an area with a certain width, what we require is simply to color a "map" with four different colors in such a way that any two adjacent regions must be painted in different colors. The well-known "four color theorem" in mathematics has already told us that this intuition is precisely correct.

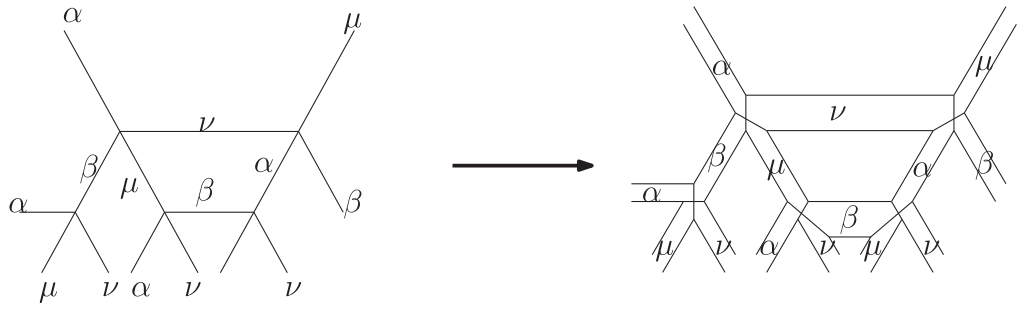

FIG. 10. The four color theorem ensures that index types α, β, μ, or ν can be unambiguously assigned to each leg in the network.

1. Calculation of entanglement entropy for a connected region

We first prove that, in this entangled thread configuration with assigned perfect tensor states, the calculation of the entanglement entropy $S(A)$ for a single connected region A satisfies the holographic RT prescription. To do this, we first calculate the reduced density matrix

$$\rho_A = \mathrm{tr}_{\bar{A}}(|\Psi\rangle\langle\Psi|), \tag{31}$$

where $|\Psi\rangle$ is now the entire tensor network state formed by gluing all perfect tensor states. Figure 11 illustrates the tensor network diagrammatic representation of the expression (31), where taking the trace over $\bar{A}$ means gluing together the indices inside $\bar{A}$. Now, we will utilize the following interesting properties of perfect tensors (depicted in Fig. 12):

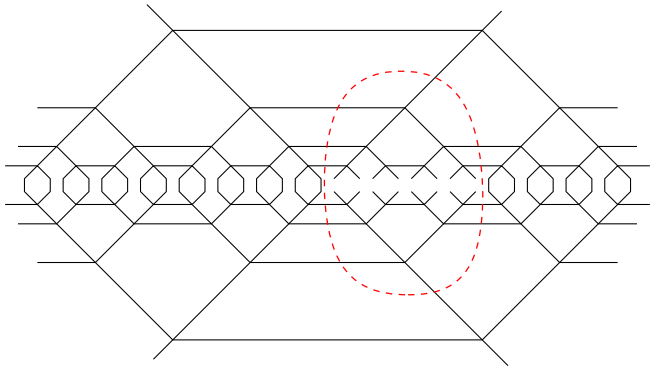

FIG. 11. The tensor network diagrammatic representation of the expression (31), where taking the trace over $\bar{A}$ means gluing together the indices inside $\bar{A}$.

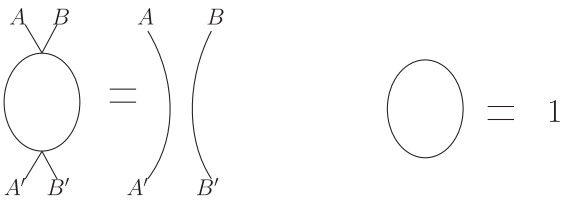

FIG. 12. The diagram representation of rules (32) and (33).

$$\sum_{\alpha\beta} T_{\alpha\beta\mu\nu}(T_{\alpha\beta\mu'\nu'})^* = \frac{1}{9}\delta_{\mu\mu'}\delta_{\nu\nu'}, \tag{32}$$

and

$$\sum_{\mu} \frac{1}{3}\delta_{\mu\mu'} = 1, \tag{33}$$

where each $1/3\delta$ represents a tensor $\begin{bmatrix} \frac{1}{3} & 0 & 0 \\ 0 & \frac{1}{3} & 0 \\ 0 & 0 & \frac{1}{3} \end{bmatrix}$, characterizing the density matrix of a single qutrit as $\rho = \sum_{i=0,1,2} \frac{1}{3}|i\rangle\langle i|$, and thus conveniently represented by a single thread. A circle then represents the trace over the tensor $1/3\delta$, yielding 1.

Applying these two simple rules iteratively, we can simplify expression (31) step by step, and all operations will be performed graphically, see Fig. 13. In the first step, we use Eq. (32), and in the second step, we use Eq. (33). By combining these two steps, we find that this process suggests that short-range entanglement from previous layers has not entered into the calculation at larger scales. Moreover, after this process, a symmetric pattern suitable for iteration emerges. We can use (32) and (33) again to further remove short-range entanglement. After repeated iterations, the net result is obtained in Fig. 13(e). Observing this result, to calculate the entanglement entropy of A, we actually only need to consider a subnetwork, which can be precisely interpreted as the entanglement wedge $W(A)$ of A. Denoting the lattice sites included in A as x_a and the sites included in the minimal cut γ_A as s_γ, this entanglement wedge subnetwork can be seen as characterizing a pure state of the whole set $\{x_a\} \cup \{s_\gamma\}$, and calculating the von Neumann entropy of A is also equivalent to calculating the entanglement entropy between $\{x_a\}$ and $\{s_\gamma\}$.

To calculate this entanglement entropy more conveniently, as shown in Fig. 14(b), we next choose to contract $\{x_a\}$ rather than $\{s_\gamma\}$. In other words, we calculate the reduced density matrix corresponding to the entanglement entropy

$$\rho_{\mathrm{ent}} = \mathrm{tr}_{\{x_a\}}(|\psi_A\rangle\langle\psi_A|), \tag{34}$$

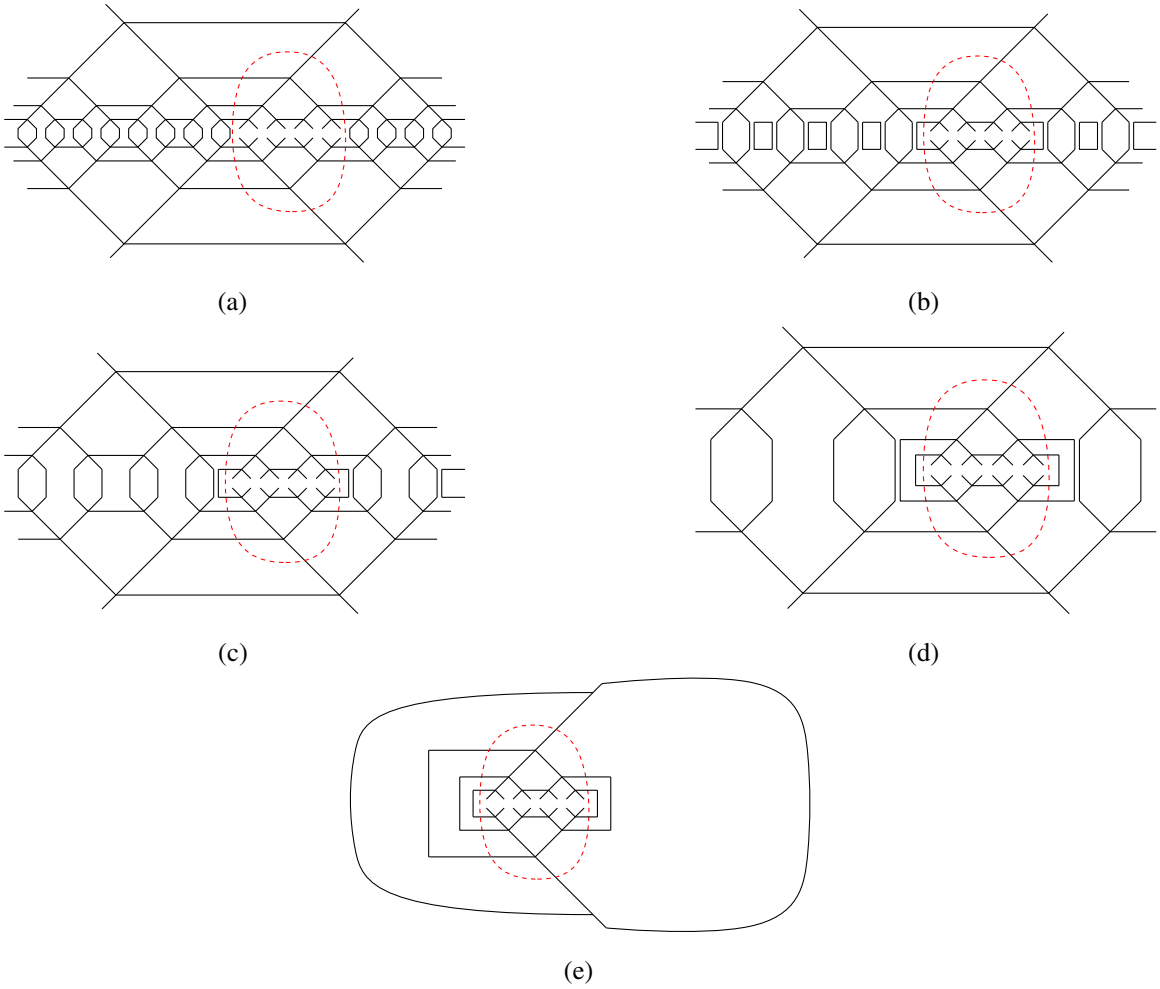

FIG. 13. (a) The original diagram representing (31). (b) The first step, in which (32) has been used. (c) The second step, in which (33) has been used. (d) Iteratively using (32) and (33) due to the symmetry. (e) The net result.

where $|\psi_A\rangle$ represents the state corresponding to the entanglement wedge subnetwork of A.

As shown in Fig. 14(c), we then iteratively apply the expressions (32) and (33) again, and finally, we find that the graphical representation of this density matrix is simply a cluster of threads representing the direct product of Bell pairs. Moreover, the number of threads is exactly equal to the number of threads crossed by the minimal cut. Thus, we verify the first expectation that coupling the thread configuration according to the entanglement pattern of perfect tensors does not affect the expression of the entanglement entropy for connected subregions. Note that, similarly, in the process of graphical calculation, it can be clearly seen that short-range entanglement within A does not contribute to the entanglement entropy of A.

2. Calculation of entanglement entropies for disconnected regions

Next, we will clarify the proof that resolves the calculation problem of entanglement entropy for disconnected regions proposed in Sec. V A. The method is similar, employing the expressions (32) and (33), with some subtle details that we present in this section.

Consider the configuration as shown in Fig. 15(a), where the entanglement entropy of $A = A_1 \cup A_2$ is given by the sum of the areas of the RT surfaces γ_1 for A_1 and γ_2 for A_2. The steps for calculating the entanglement entropy are similar. Again, we first calculate the reduced density matrix ρ_A by gluing together the indices inside $\bar{A}$. Then, we iteratively apply the two simple rules (32) and (33) to simplify the expression (31). The first and second steps are illustrated in Fig. 15. Similarly, symmetry allows an iterative scheme, and we can proceed similar to Fig. 14(c). It can be verified that, by iterating continuously, the final pattern in Fig. 15(d) is obtained.

Note that, in the current context, although during the iteration process entanglement at each scale has been removed by (32) and (33), some long-range entanglement crossing the disconnected regions A_1 and A_2 has not been removed. This is manifested in the pattern as circles around A_1 and A_2. Let us denote these circles from inner to outer as

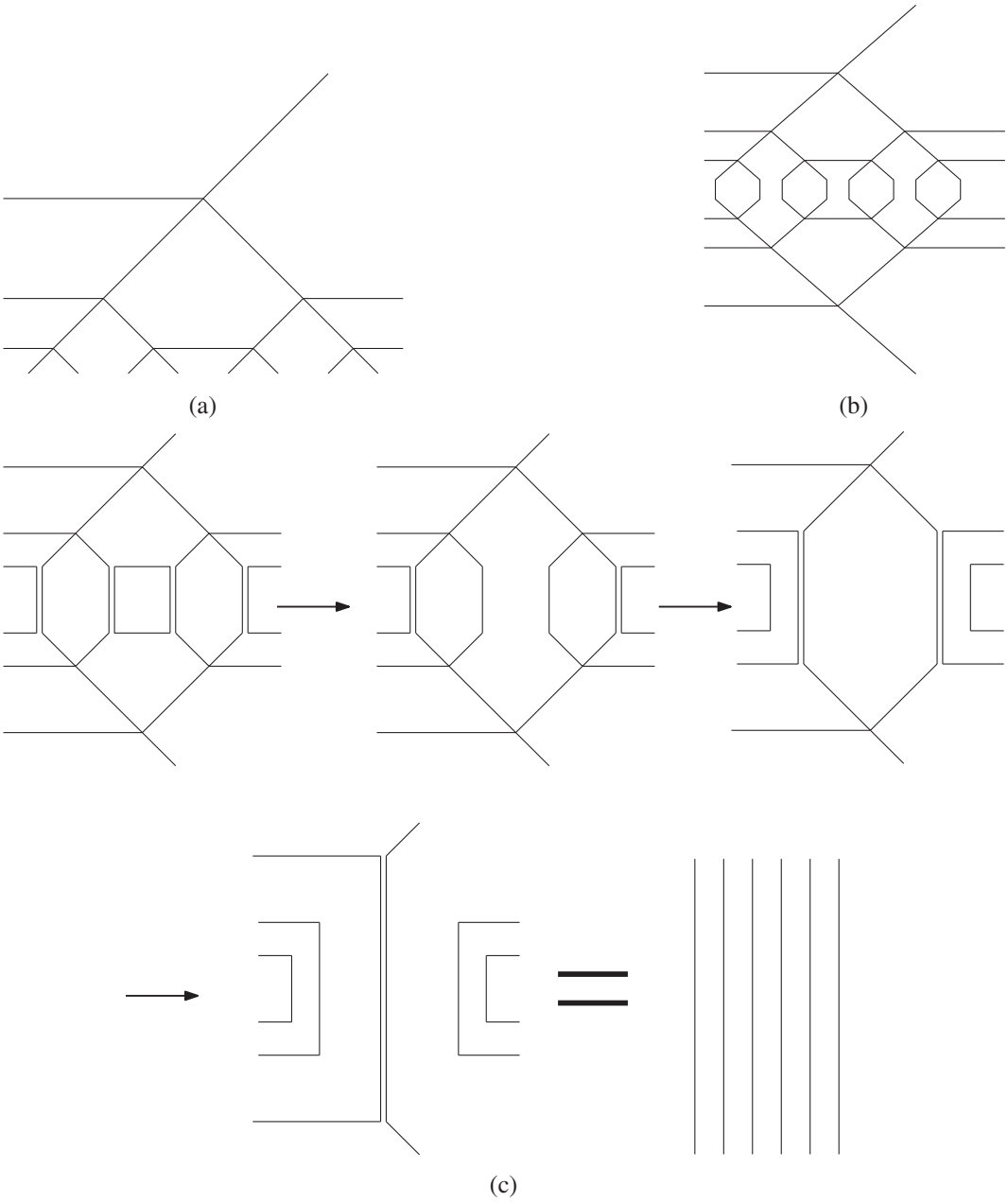

FIG. 14. (a) Figure 13(e) tell us that to calculate $S(A)$ we only need to consider a subnetwork. (b) Equivalently calculate the entanglement entropy between $\{x_a\}$ and $\{s_\gamma\}$. (c) Iteratively applying (32) and (33) finally leads to a simple result.

$C_1, C_2, \ldots, C_n$, where these circles intersect only at circles O_1 surrounding A_1 or circles O_2 surrounding A_2. Note that more outer circles have already been removed by the previous standard procedure through (32) and (33).

However, we can further eliminate circles $C_1, C_2, \ldots, C_n$ using (32) and (33). As shown in Fig. 16, we first apply (32) at the intersection of the outermost circle C_n with either O_1 or O_2, and the net result is the decoupling of the circle C_n from O_1 and O_2, i.e., they no longer intersect. Therefore, by (33), C_n no longer contributes to the entropy calculation. Obviously, this process can be repeated, successively removing $C_{n-1}, \ldots, C_1$, until reaching the final configuration in Fig. 15(d).

To handle the final configuration in Fig. 15(d), note that it is topologically equivalent to the configuration in Fig. 16(a). Thus, as shown in Fig. 16, we can first apply (32) and then (33) to reach the configuration in Fig. 16(c). However, Fig. 16(c) is nothing else but the sum of the entanglement entropy for regions A_1 and A_2, and the entanglement entropy for A_1 and A_2 is precisely given by the number of cuts through their respective entanglement wedges. We can replicate the calculation in Fig. 14(c)

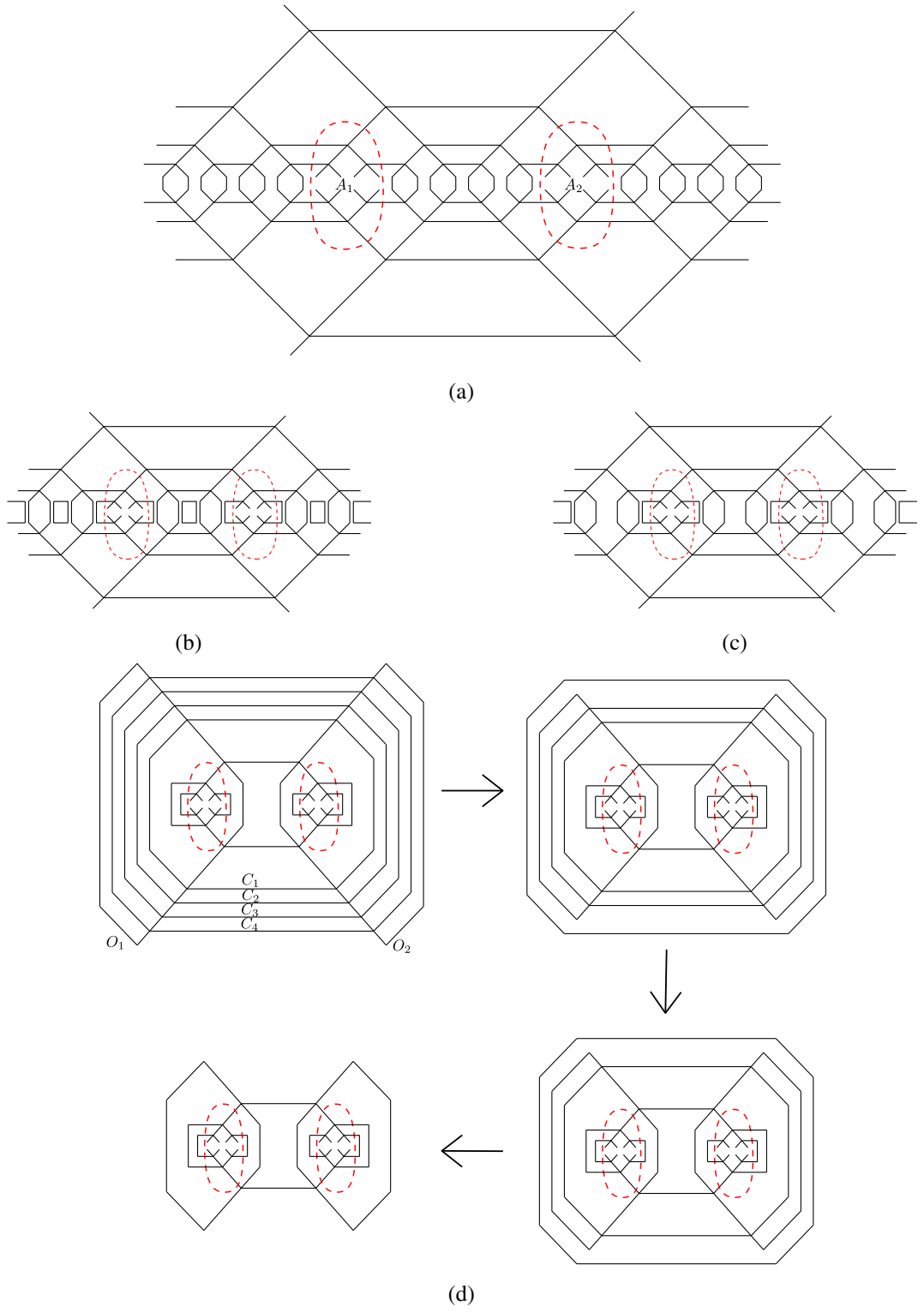

FIG. 15. Calculation of entanglement entropy for a disconnected region. (a) The reduced density matrix of a disconnected region. (b) The first step of calculation. (c) The second step of calculation. (d) By iterating, the final pattern is obtained.

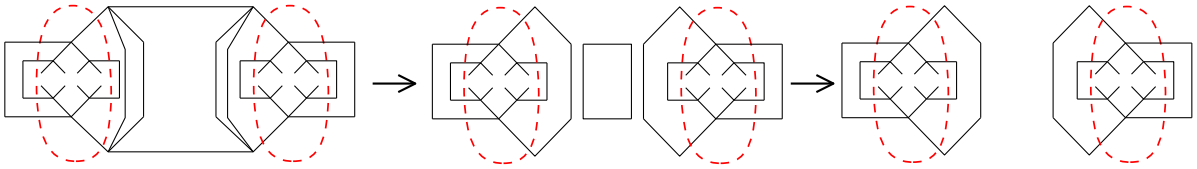

FIG. 16. Calculation of entanglement entropy for a disconnected region.

and obtain the following result:

$$S(A_1 \cup A_2) = k \ln 3(\text{No. cut}_{\gamma(A_1)} + \text{No. cut}_{\gamma(A_2)}). \quad (35)$$

Thus, we obtain

$$S(A_1 \cup A_2) = S(A_1) + S(A_2), \quad (36)$$

where "No. $\text{cut}_{\gamma(A_1)}$" represents the number of cut legs through the minimal surface $\gamma(A_1)$. k is a coefficient chosen as needed.

Note that, according to this, the paradox proposed in Sec. III A has received an insightful resolution. In our case, there indeed exists a thread [the green thread shown in Fig. 15(a)] that characterizes the conditional mutual information between regions A_1 and A_2. If we simply interpret this CMI as a kind of bipartite entanglement, we cannot consistently characterize (36). But now we consider this thread as being in an entangled state with other threads, and we have just proven that this entanglement scheme allows the characterization of entanglement entropy for disconnected regions.

Now, for completeness, we should also prove that this perfect tensor-type thread configuration can give another facet of entropy for disconnected subregions. As is well known, for a disconnected subregion $A = A_1 \cup A_2$, the holographic RT surface can be either $\gamma(A_1) \cup \gamma(A_2)$ or $\gamma(A_1 \cup L \cup A_2) \cup \gamma(L)$, where L is the intermediate region between A_1 and A_2, as long as the latter gives a smaller area. Figure 17(a) shows an example of this situation, noting that there are still threads connecting A_1 and A_2 that characterize the conditional mutual information relative to L. It now needs to be proved that, in this case, counting the number of cut legs still correctly gives the entanglement entropy, i.e., prove

$$S(A_1 \cup A_2) = S(A_1 \cup L \cup A_2) + S(L), \quad (37)$$

or

$$S(A_1 \cup A_2) = k \ln 3(\text{No. cut}_{\gamma(A_1 \cup L \cup A_2)} + \text{No. cut}_{\gamma(L)}). \quad (38)$$

Based on the previous calculation experience, we can now easily go from the original configuration of calculating

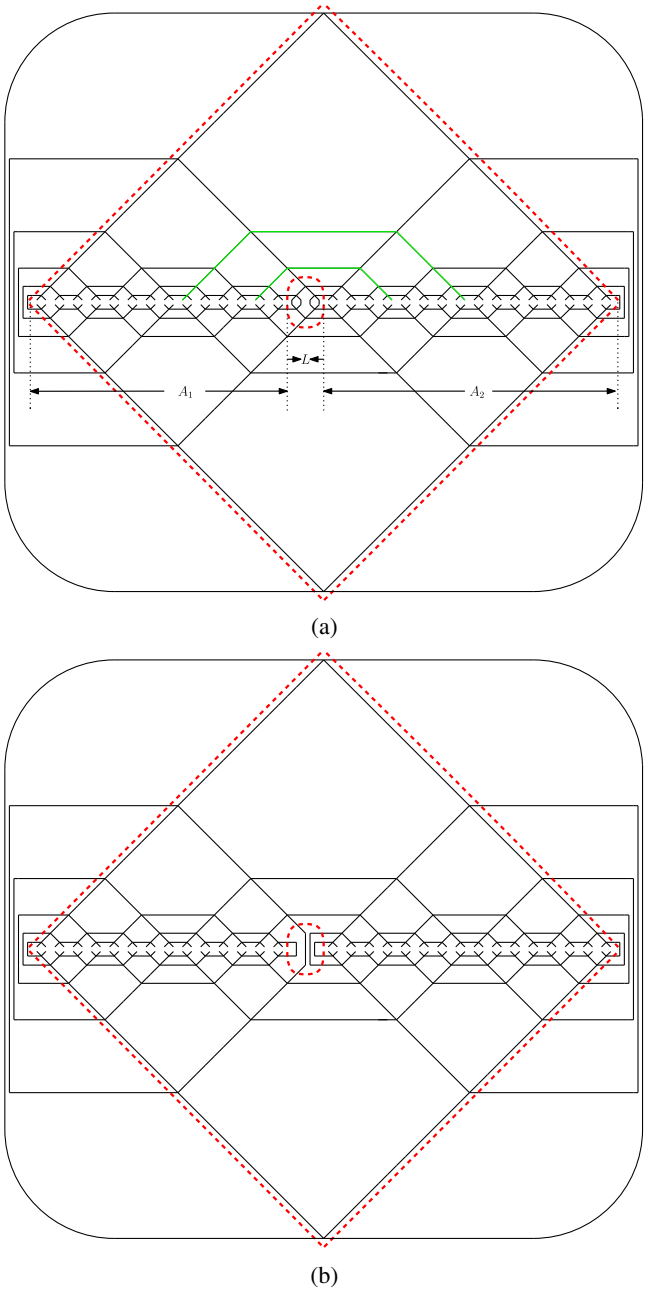

(a)

(b)

FIG. 17. (a) The reduced density matrix for another case of disconnected region's entanglement entropy. (b) First reduce the thread configuration inside $\gamma(L)$.

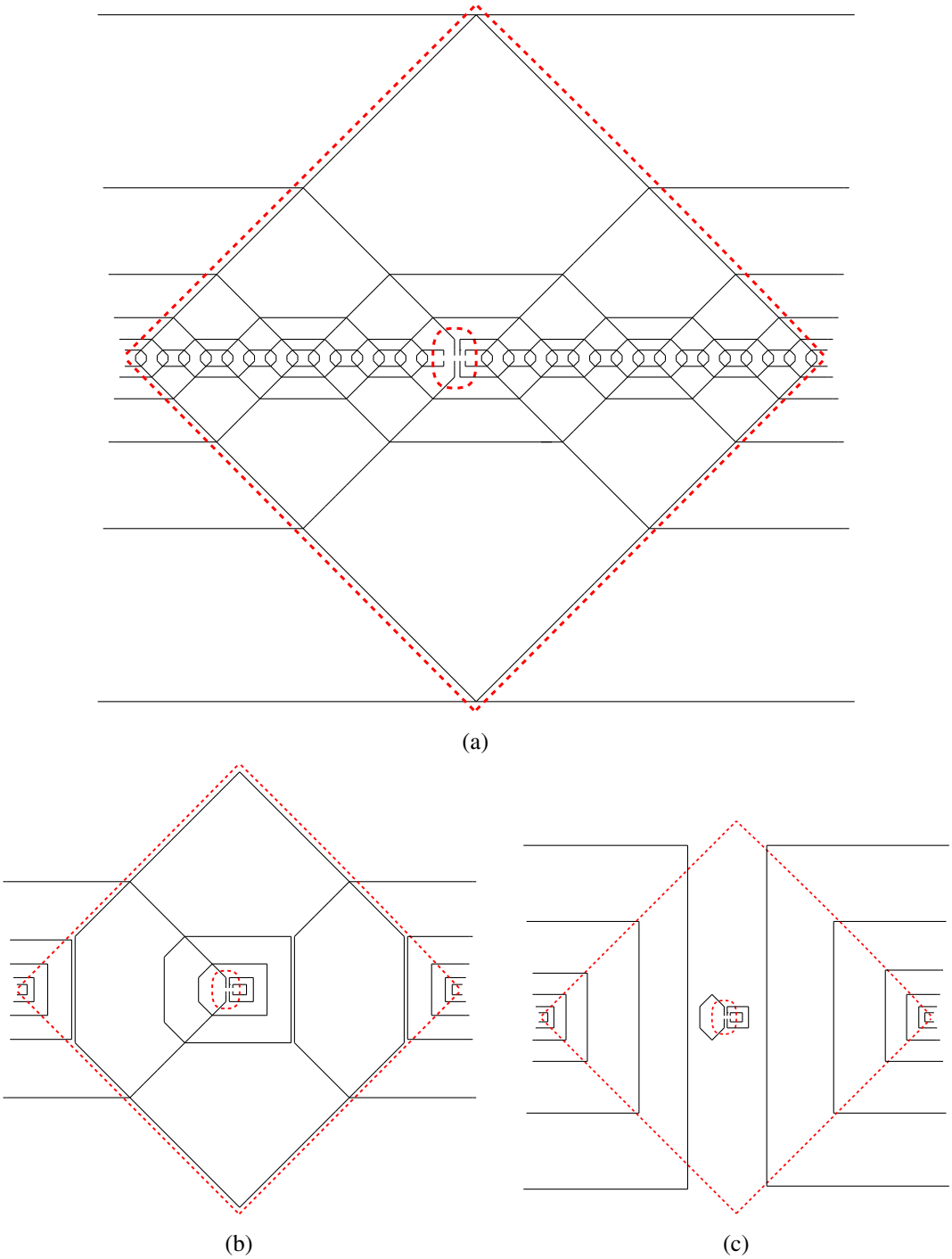

FIG. 18. The calculation details. (a) Calculation equivalent to Fig. 18(a). (b) The pattern obtained by a series of reductions. (c) The final pattern.

the reduced density matrix ρ_A directly to the pattern in Fig. 17(a). This is because we can continuously use (32) and (33) to reduce the threads and circles outside the surface $\gamma(A_1 \cup L \cup A_2)$ to the configuration in Fig. 17(a). On the other hand, from the calculation in Fig. 12, we can also directly reduce the thread configuration inside the surface $\gamma(L)$ to the configuration in Fig. 17(b).

Following a similar logic to the step in Fig. 14(b), now Fig. 17(b) is equivalent to calculating Fig. 18(a). Thus, we arrive at a pattern that is very easy to directly apply (32) and (33) for reduction, and after several steps of operation, we get the pattern in Fig. 18(b). Making a deformation that preserves the topology, we can continue to use (32) and (33), thus finally obtaining Fig. 18(c). Figure 18(c)

consists of two parts, where the smaller part, by a calculation similar to Fig. 13(e), will contribute to $S(L)$, and the other part precisely calculates the entanglement entropy of the reduced density matrix represented by n threads, where n is precisely proportional to $\gamma(A_1 \cup L \cup A_2)$. Thus, we have completed the proof.

VI. CHARACTERIZATION OF ENTANGLEMENT WEDGE CROSS SECTIONS

A. Review of entanglement of purification

In the holographic duality, there exist many quantum information theory quantities that characterize the correlations between subsystems A_1 and A_2 in a mixed-state bipartite system $A = A_1 \cup A_2$. Here, we choose to use the entanglement of purification $E_P(A_1:A_2)$ [97,98] to characterize this correlation. The method is as follows: imagine introducing two auxiliary systems, denoted as A_1' and A_2', so that $A_1 \cup A_2 \cup A_1' \cup A_2'$ as a whole is in a pure state $\psi(A_1A_2A_1'A_2')$. In this way, one can legitimately define the entanglement entropy between A_1A_1' and A_2A_2'. As there are infinitely many purification schemes, the entanglement of purification takes the minimum entanglement entropy $S(A_1A_1')$ between A_1A_1' and A_2A_2' over all possible schemes as the correlation between A_1 and A_2, i.e.,

$$E_P(A_1:A_2) = \min_{|\psi\rangle_{A_1A_1'A_2A_2'}} S(A_1A_1'). \tag{39}$$

Similar to the RT formula, it has been proposed in the literature [97,98] that the entanglement of purification can be calculated from the area of the dual EWCS surface, i.e.,

$$E_P(A_1:A_2) = \frac{\mathrm{Area}(\sigma_{A_1:A_2})}{4G_N}. \tag{40}$$

Detailed discussions on holographic entanglement of purification are found in the literature on surface-state duality (see [74,110,111]). Since what we want to measure is the (minimal possible) entanglement entropy between A_1A_1' and A_2A_2', the optimal scheme should first satisfy that the auxiliary system $A_1' \cup A_2'$ itself has no internal entanglement, allowing its Hilbert space to be used most economically, thus providing a purification with the smallest possible Hilbert space dimension. Intuitively, the dimension of the Hilbert space of $A_1' \cup A_2'$ with no internal entanglement is precisely used entirely to characterize the entanglement between A_1 and A_2, thereby capturing the intrinsic correlation between A_1 and A_2.

B. Necessity of perfect entanglement for mixed-state intrinsic correlations

Let us choose A_1 and A_2 as shown in Fig. 19, and we have marked the types of various threads with colors in the figure. Before "tying up" all the threads (corresponding to the original direct-product coarse-grained state), we can see that the green threads represent the connections between A_1 and A_2, the yellow threads represent the connections from A_1 to the region we define as B_2, and the purple threads represent the connections from A_2 to the region we define as B_1. Note that we have arranged for the number of yellow threads to be equal to the number of purple threads. In other words, we have agreed on B_1 and B_2 in such a way that

$$N_{A_1\leftrightarrow B_2} = N_{A_2\leftrightarrow B_1}. \tag{41}$$

Thus, we obtain a configuration consistent with Sec. III B. We can also precisely draw the position of the entanglement wedge cross section in the current context. It is the minimal cut (indicated by red solid line in the figure) that starts from the boundary point of A_1 and A_2 and divides the entanglement wedge $W(A_1 \cup A_2)$ into two halves. In this setup, we can reproduce the "experimental results" (15): Given

$$N_{A_1\leftrightarrow A_2} = 1, \tag{42}$$

$$N_{A_1\leftrightarrow B_2} = N_{A_2\leftrightarrow B_1} = 2, \tag{43}$$

$$\frac{\mathrm{Area}(\sigma_{A_1:A_2})}{4G_N} = \text{No. minimal cut} = 3, \tag{44}$$

we have

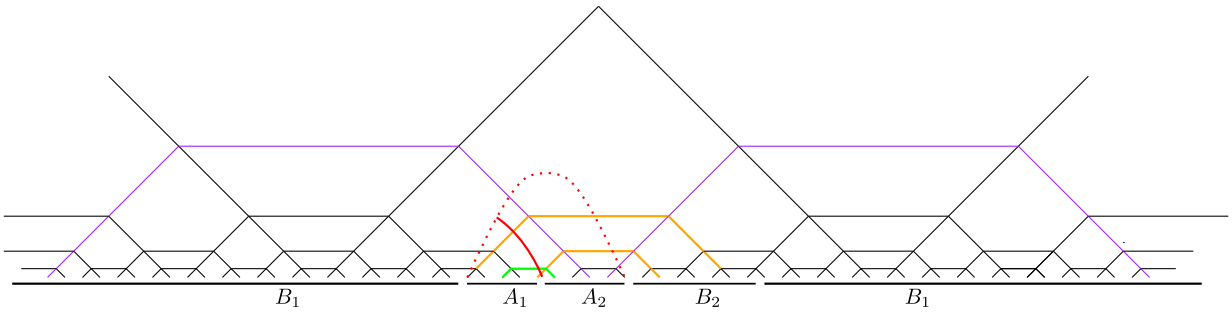

FIG. 19. Here the entanglement wedge cross section is the minimal cut indicated by the red solid line. We have arranged for the number of yellow threads to be equal to the number of purple threads, which means $N_{A_1\leftrightarrow B_2} = N_{A_2\leftrightarrow B_1}$.

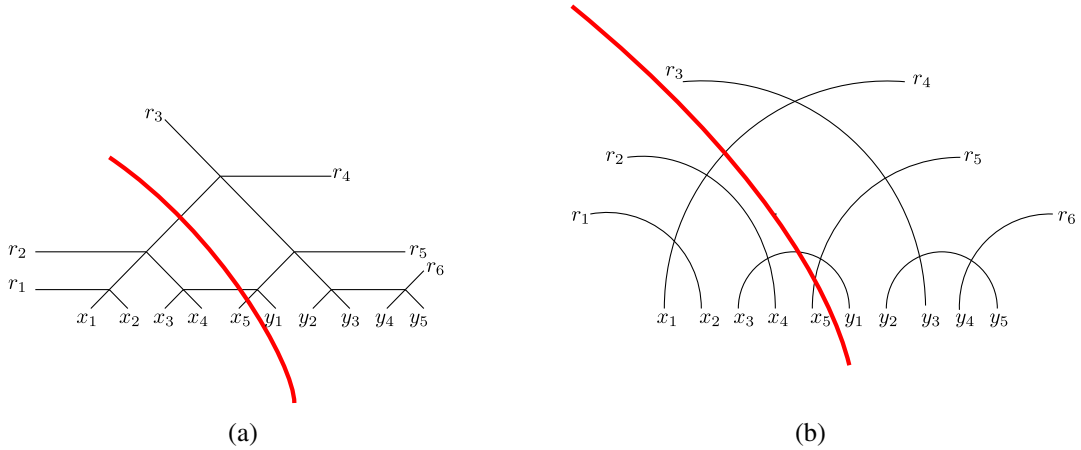

FIG. 20. (a) The entanglement wedge of $A = A_1 \cup A_2$, the red solid line represents EWCS. (b) the minimal entanglement of purification when the coarse-grained state is simply obtained by the direct product of all threads.

$$\frac{\text{Area}(\sigma_{A_1:A_2})}{4G_N} = N_{A_1\leftrightarrow B_2} + N_{A_1\leftrightarrow A_2} = N_{A_2\leftrightarrow B_1} + N_{A_1\leftrightarrow A_2}. \tag{45}$$

Consider the case where $A = A_1 \cup A_2$ as a whole is a connected region. Recall that in Sec. V B, we have obtained a tensor network representation of the reduced density matrix of any connected region, as shown in Fig. 14(b), which is the adhesion of the entanglement wedge and its mirror image. In this section, we label the sites inside A_1 as x_i, the sites inside A_2 as y_j, and the sites contained in the minimal cut γ_A of A as r_k. In particular, we have chosen a concise example as shown in Fig. 20, where

$$A_1 = \{x_1, x_2, x_3, x_4, x_5\}. \tag{46}$$

As pointed out in Sec. V B, the minimal cut γ_A can be regarded as a purification of the system $A = A_1 \cup A_2$. In other words, the system $\gamma_A \equiv \{r_k\}$ can be exactly regarded as the auxiliary system $A_1' \cup A_2'$. The resulting purified state $\psi(A_1A_2A_1'A_2')$ is precisely the state $|\psi_A\rangle$ corresponding to the entanglement wedge subnetwork of A. More importantly, when tracing out A from $|\psi_A\rangle$, we obtain that the reduced density matrix of γ_A is direct product (see Fig. 14), in other words, it does not contain internal entanglement. Therefore, the auxiliary system $\gamma_A = A_1' \cup A_2'$ can now be used to characterize the intrinsic correlation between A_1 and A_2.

If we regard the thread configuration simply as the direct product of all threads representing Bell states, how much is the intrinsic correlation between A_1 and A_2? For this, we can partition the sites in γ_A as follows to obtain the minimal entanglement of purification $S(A_1A_1' \leftrightarrow A_2A_2')$ as a measure of this intrinsic correlation,

$$A_1' = \{r_1, r_2, r_4, r_5\}, \qquad A_2' = \{r_3, r_6\}. \tag{47}$$

How do we know this is the optimal solution? Notice that x_1 forms the Bell pair with r_4 that has the maximum entanglement, and x_5 forms the Bell pair with r_5, and so on. The principle is to try to place pairs of sites with maximum entanglement into the same group. In this way, what truly characterizes the intrinsic correlation between A_1 and A_2 is only one Bell pair, which is represented by the thread connecting x_3 and y_1. Any other nonoptimal purification scheme would introduce redundant correlations. For example, if we factitiously consider sites r_4 and r_5 as degrees of freedom belonging to A_2', it would introduce redundant correlations between A_2' and sites x_1, x_5 in A_1. In a word, as implicitly implied in Sec. III B, when using a coarse-grained state containing only bipartite entanglement, that characterizes the intrinsic correlation between A_1 and A_2 is only the number $N_{A_1\leftrightarrow A_2}$ of threads directly connecting A_1 and A_2 (such as x_3 connecting to y_1),

$$E_P(A_1:A_2) = \min_{|\psi\rangle_{A_1A_1'A_2A_2'}} S(A_1A_1') = N_{A_1\leftrightarrow A_2}, \tag{48}$$

and this equation contradicts (45).

This is not a mathematical difficulty but signifies a rigid physical requirement: we must introduce ingredients beyond bipartite entanglement. The perfect entanglement scheme can indeed resolve this physical dilemma. As shown in Fig. 21(a), let us verify the expected optimal purification scheme from the surface-state duality, i.e.,

$$A_1' = \{r_1, r_2\}, \qquad A_2' = \{r_3, r_4, r_5, r_6\}. \tag{49}$$

By this, we perform the calculation of the entanglement entropy $S(A_1A_1' \leftrightarrow A_2A_2')$, which means tracing

$$\rho_{A_1A_1'} = \text{tr}_{A_2A_2'}\psi(A_1A_2A_1'A_2'). \tag{50}$$

The graphical algorithm is shown in Fig. 21(a). Similarly, at a particular step, we can again use the technique of

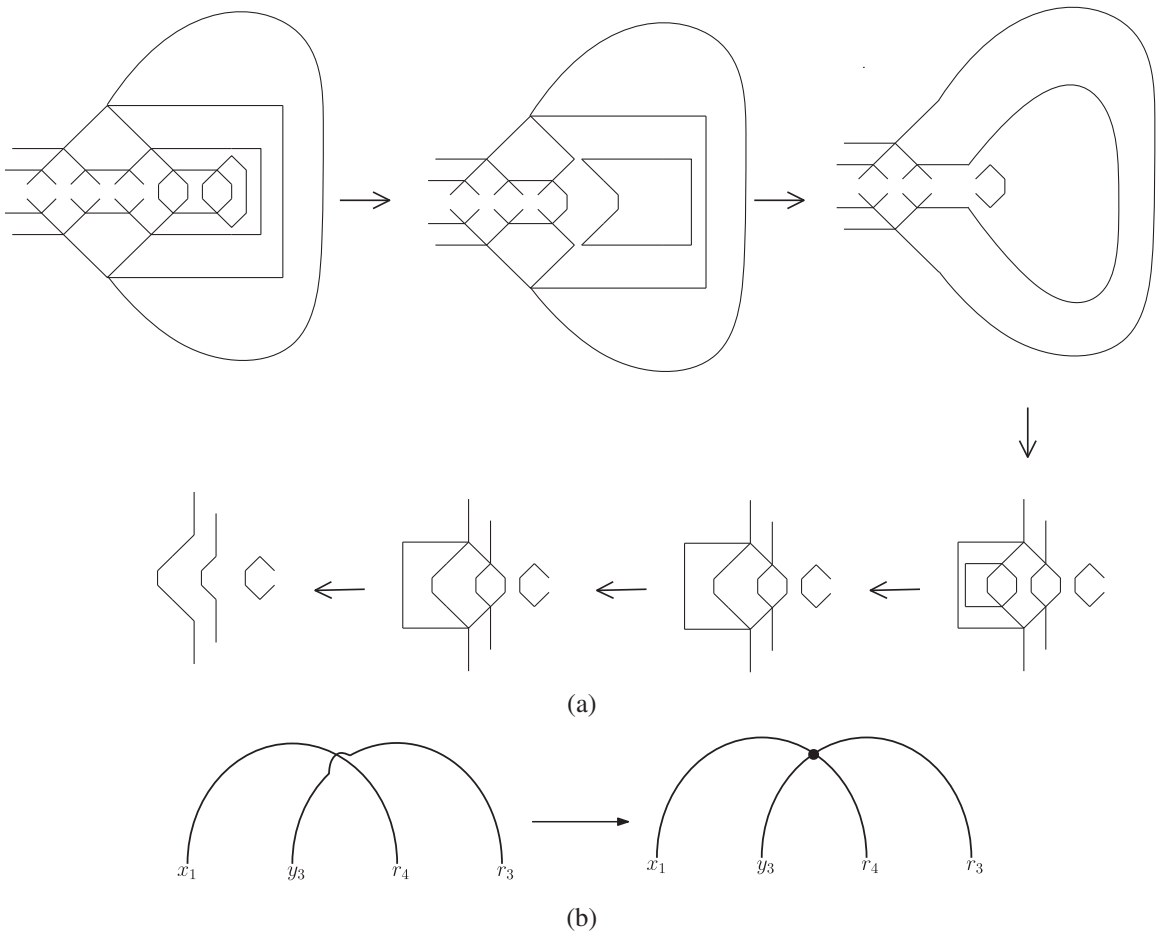

FIG. 21. (a) The calculation of the entanglement entropy $S(A_1A_1' \leftrightarrow A_2A_2')$ according to the optimal purification scheme expected from the surface-state duality. (b) The introduction of perfect entanglement.

exchanging the trace to calculate the entanglement entropy. The ultimately simplified net result consists of three direct-product threads, which gives the correct answer (44). Interestingly, we can also identify from the figure that the sources of these three threads exactly correspond to all the green and purple threads in Fig. 19. Readers can also verify that, if the purification scheme (47) is adopted, a larger entropy will be obtained.

Although we have presented a detailed calculation, it is not difficult to straightforwardly grasp the most essential nature. Seeing Fig. 21(b), focusing on the site $x_1 \in A_1$ and the site $y_3 \in A_2$, before applying perfect entanglement to the coarse-grained state, there is obviously no entanglement between x_1 and y_3. Therefore, it cannot contribute to the correlation between A_1 and A_2. However, after coupling the thread $\zeta_{x_1 r_4}$ and the thread $\zeta_{y_3 r_3}$ into a perfect tensor state, x_1 and y_3 are locally living in a full entangled state. At this point, we must find a way to measure the intrinsic correlation between x_1 and y_3. A natural way is entanglement of purification, and the optimal purification scheme is to choose $r_3 \cup r_4$ as the auxiliary system associated with y_3 and choose the empty set as the auxiliary system associated with x_1. In this way, the amount of entanglement obtained will be $1 \times \log 3$.

C. Discussion on more general thread configurations

Attentive readers will notice a particular feature in Fig. 1(c): it only presents nonintersecting RT surfaces (in the context of tensor network, this implies considering tree tensor networks [17,52]). Indeed, in the current study of thread configurations, we mainly focus on the characteristics of fluxes of thread bundles. What about the specific details of how these threads traverse through the bulk?

The study of entanglement wedge cross sections, which are extremal surfaces whose end points can be located within bulk, indicates that we can go further. As shown in Fig. 22, we can consider two boundary subregions B_1 and B_2 with overlaps, denoting their overlap region as A_2, and let $A_1 = B_1 \backslash A_2$ and $A_3 = B_2 \backslash A_2$, with the remaining part of the system denoted as A_4. Correspondingly, denote the RT surfaces of B_1 and B_2 as γ_{12} and γ_{23}. Inevitably, γ_{12} and γ_{23} intersect. At this point, if we focus on the overlapping region A_2 and consider the thread bundles from A_2 to A_4, we find two possible scenarios: threads can either first pass

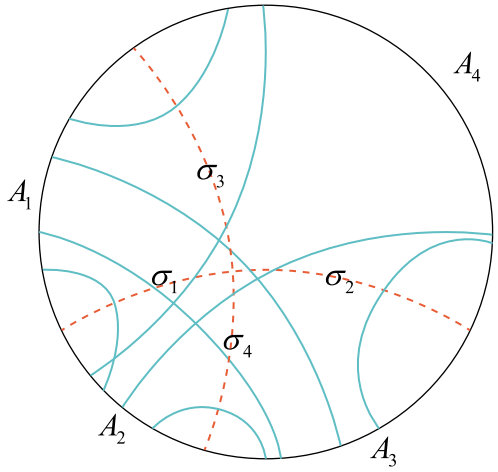

FIG. 22. A more refined thread configuration.

through the σ_1 surface in the diagram and then reach A_4, or they can first pass through the σ_2 surface and then reach A_4. On the other hand, if we consider the threads from A_2 to A_1, we would have reason to believe that these threads must all pass through the σ_1 surface to enter A_1. In other words, threads from A_2 passing through the σ_2 surface before reaching A_1 are not allowed. This straightforwardly inherits the experience from bit threads [53–56]. Simply put, under the requirements of bit threads, the maximum number of bit threads connecting two complementary connected regions must equal the minimum area of the bulk surface (i.e., RT surface) that separates these two regions. This is known as the max-flow min-cut theorem. Since bit threads are required not to exceed a constant density $\frac{1}{4G_N}$ in the bulk, if a thread crosses the RT surface twice or more, it will occupy the positions of the threads connecting the two complementary regions, thus preventing the maximization of the number of threads. On the other hand, due to the overly strict constraints of the original thread density of bit threads, there are significant obstacles to the existence of thread configurations (see the detailed discussion in Ref. [57]), therefore, we only retain this topological property of the threads: an internal thread connecting two subsystems within a connected region (such as B_1 here) should not overflow its corresponding RT surface (such as γ_{12} here), or in other words, an internal thread of a connected region will not pass through its RT surface more than once. It is worth noting that this also aligns well with the spirit of entanglement wedge reconstruction of boundary subregions [112–117]. If we attribute possible quantum information-theoretic meanings to such threads, the bulk information "decoded" from the information of a subregion should still lie within its entanglement wedge. We believe that the thread-state correspondence [61–63] mentioned in this paper is a simple and inspiring attempt to take this idea seriously, where not only the end points of a thread connecting two boundaries, but also the "bulk sites" on the RT surfaces that the thread traverses through are considered to correspond to some qudits, and together form a special entangled quantum state indicated by the thread.

For the simple example in Fig. 22, we can easily enumerate all independent thread bundles. Recall that, for the four elementary regions A_1, A_2, A_3, A_4, we previously had a total of $\frac{4\times3}{2}=6$ independent thread bundles, which consequently yield six unknown fluxes N_{ij} to be solved, where the subscripts ij range from 1 to 4. The entanglement entropy of the six connected regions (i.e., the area of their RT surfaces) then exactly provides six constraints, ensuring a full rank solvable linear equation system. As shown in Fig. 22, however, now we can find a total of eight independent thread bundles, simply because two of them have split. Their flux relations can be explicitly expressed as

$$\begin{aligned} N_{13} &= N_{13}^{\sigma_1\sigma_4} + N_{13}^{\sigma_3\sigma_2}, \\ N_{24} &= N_{24}^{\sigma_1\sigma_3} + N_{24}^{\sigma_4\sigma_2}, \end{aligned} \tag{51}$$

where superscripts indicate the intermediate surfaces encountered along the thread. In principle, adding two new unknown fluxes implies the need for the areas of two new additional surfaces as constraints. Obviously, the areas of the σ_1 and σ_3 surfaces can serve as choices. Note that, since the areas of all RT surfaces of connected regions have already been used, once the area of σ_1 is determined, the area of σ_2 is also determined. Similarly, the area of σ_4 is no longer a new constraint. Next, similar to (4), we only need to track the threads passing through these independent surfaces and require the number of threads to match the area of the surfaces to obtain the complete system of equations. The key point is that this approach provides an idea for more refined thread configurations. We can consider more complex scenarios involving more intersecting RT surfaces, where the RT surfaces are divided into more components. By "more refined," we mean that, in addition to knowing the information about the thread fluxes connecting various boundary elementary regions, one can also further know how much proportion of threads pass through different parts of RT surfaces in the bulk. We will systematically study the more general and refined thread configurations in another work [118], using the tools of kinematic space.

Furthermore, a natural question arises: Can this more refined thread configuration further be used to provide (or "detect") information about the entanglement structure of holographic dualities? A possible idea is to associate it with the concept of differential entropy [119–121]. The reason is that differential entropy has been proposed to characterize the area of arbitrary surfaces within the holographic bulk, while in the context involving more refined thread configuration, we have gone beyond the discussion of RT surfaces anchored to the boundary; that is, we can extend the thread method to more general bulk extreme surfaces. Therefore, by associating more general thread

configurations with the idea of differential entropy in the context of quantum information theory, it is possible to obtain more interesting results about the entanglement structure of holographic dualities. We leave this aspect of the research for future exploration.

VII. CONCLUSION AND DISCUSSION

In recent years, many concepts and tools from quantum information theory have been employed to study the quantum entanglement structure in holographic duality. It is extremely challenging to directly derive the mechanism that precisely generates the quantum entanglement structure of the dual spacetime in one fell swoop. Therefore, we choose to explore this entanglement structure at a coarse-grained level, which has generated some insightful and crucial clues. More specifically, we focus on a core concept: conditional mutual information, constructing a class of coarse-grained states intuitively related to a family of thread configurations. It is noteworthy that such coarse-grained states are closely connected to concepts such as kinematic space, holographic entropy cone, holographic partial entanglement entropy, and so on. However, fundamentally, these coarse-grained states are just direct-product states of bipartite entangled states. When we attempt to use these coarse-grained states to further characterize some quantum information theory quantities with geometric duals in holographic duality, such as entanglement entropy of disconnected regions and entanglement of purification dual to entanglement wedge cross section, unavoidable difficulties arise even at the coarse-grained level. On the other hand, introducing perfect tensor entanglement with permutation symmetry naturally solves these problems.

In summary, there are several notable findings in this paper. First, our work, in a sense, provides a equivalency between two quantum information theory quantities of entanglement wedge cross section—entanglement of purification and balanced partial entropy [i.e., expression (15)]. This relies on our physical interpretation of replacing bipartite entanglement with perfect entanglement. Before this, expression (15) should be regarded as a noteworthy "experimental phenomenon." Only when adopting this understanding of perfect entanglement can expression (15) reasonably characterize the intrinsic correlation between two parts of a system in a mixed state. Second, we re-examine, in a sense, the connection between MERA structure and kinematic space. We construct a coarse-grained state with MERA structure, and it is noteworthy that this coarse-grained state does not need to completely characterize the ground state of the holographic CFT, but only delineates its entanglement structure at the coarse-grained level. However, this structure is already sufficient to present the key features of kinematic space: its volume density is precisely given by conditional mutual information. Moreover, our investigation indicates that the spatial points in kinematic space should not be viewed as being direct product but, in some sense, entangled together by perfect entanglement. Additionally, the thread configurations with MERA structure that we construct have an insightful role in the relation between MERA tensor networks and bit threads. In this paper, we have not considered the context of Banados-Teitelboim-Zanell (BTZ) black holes [9,25,122,123]. A very natural idea is to further consider the thread configurations dual to the MERA structure of dual BTZ black holes and their corresponding coarse-grained states. What is more intriguing is that wormhole geometry has been argued to be closely related to entanglement wedge cross section [110,111], stemming from the fact that BTZ black holes can be viewed as quotients of AdS space. Thus, we expect to once again see the necessity of perfect entanglement in the context of BTZ black holes, which may appear in a more nontrivial way. We leave this fascinating idea for future work.

APPENDIX: BASIC RULES FOR TENSOR DIAGRAM CALCULUS

This paper involves a significant amount of tensor diagram calculus. Therefore, here are some brief rules for computing with tensor networks.

We can represent a normalized quantum state over k sites (or qudits) as a simple diagram T, which consists of k legs extending from a vertex,

$$|\chi\rangle = T_{\alpha_1\alpha_2\cdots\alpha_k}|\alpha_1\alpha_2\cdots\alpha_k\rangle. \tag{A1}$$

In Fig. 23(a), we depict the case of $k = 4$, which is the primary case used in this paper. Accordingly, each end point α_i of the legs of T represents a qudit equipped with a Hilbert space of dimension d_i. With this, the tensor contraction operation can be translated into diagrammatic calculations involving T. For example, consider the operation

$$|\psi\rangle = T_{\alpha_1\alpha_2\alpha_3\alpha_4}T_{\beta_1\alpha_2\beta_3\beta_4}|\alpha_1\alpha_3\alpha_4\beta_1\beta_3\beta_4\rangle, \tag{A2}$$

for which the graphical representation is shown in Fig. 23(b), where the index contractions are represented by two corresponding legs being glued together into an inner leg. Thus, by continually gluing basic patterns, one can obtain more complex pure states of a large number of qudits.

The above procedure can be extended to operations involving density matrices. Taking the example of the state (A1) for $k = 4$, its corresponding density matrix, shown in Fig. 23(c), is

$$\rho = T_{\alpha\beta\mu\nu}T_{\alpha'\beta'\mu'\nu'}|\alpha\beta\mu\nu\rangle\langle\alpha'\beta'\mu'\nu'|. \tag{A3}$$

Because of the apparent symmetry, we represent it as the original tensor network representing a pure state accompanied by its mirror image. Additionally, to distinguish it

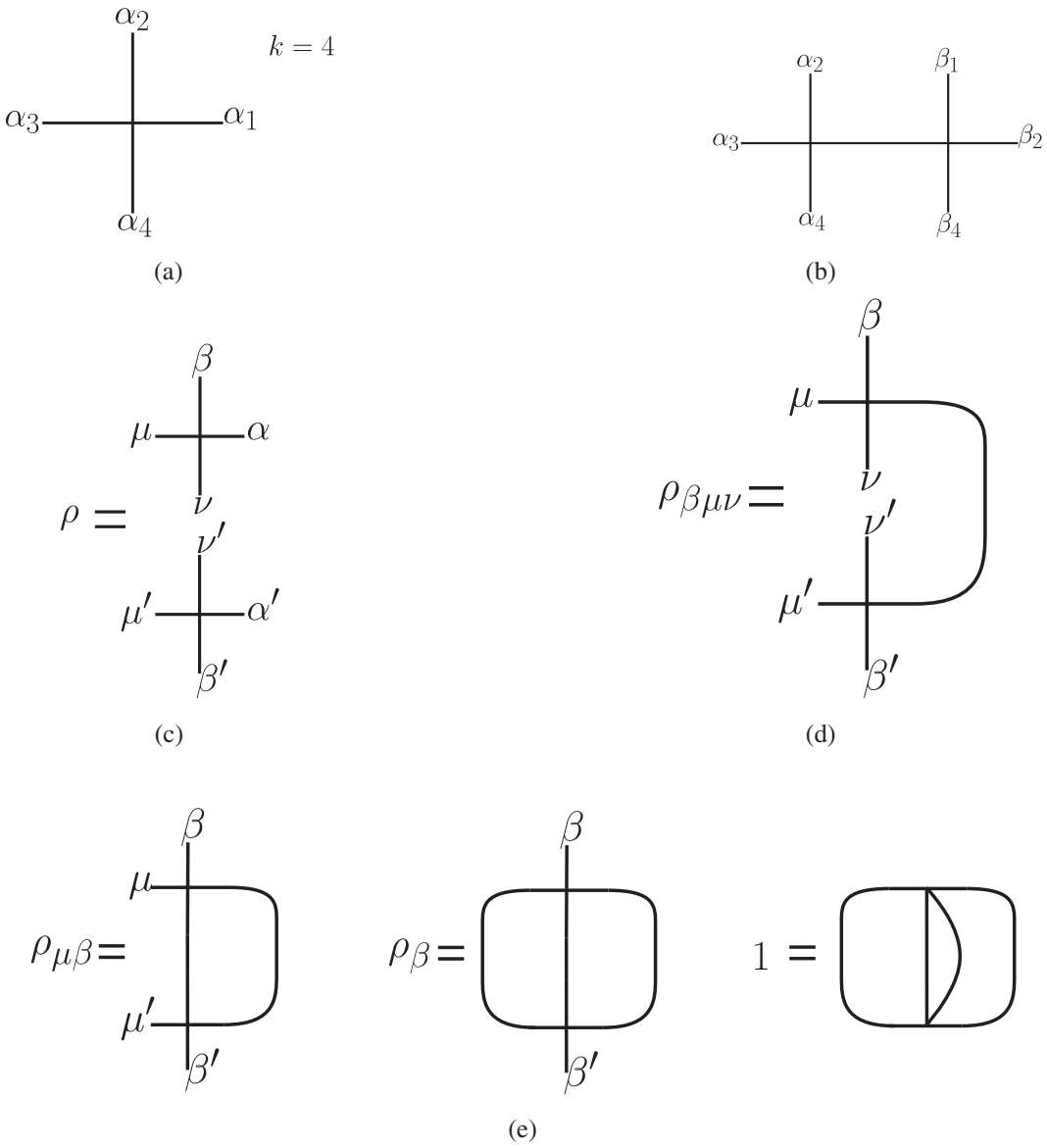

FIG. 23. Basic rules for tensor diagram calculus. (a) A tensor as a simple diagram. (b) Tensor contraction. (c) A density matrix. (d) A reduced density matrix. (e) Other examples.

from the representation of the pure state, we arrange it in an upper-lower configuration.

Now, what is interesting is that the operation of taking the trace of the density matrix becomes a diagrammatic calculation. For instance, the reduced density matrix

$$\rho_{\beta\mu\nu} = \mathrm{tr}_\alpha \rho = \sum_{\alpha''} \langle \alpha'' | \rho | \alpha'' \rangle = T_{\alpha''\beta\mu\nu} T_{\alpha''\beta'\mu'\nu'} |\beta\mu\nu\rangle\langle\beta'\mu'\nu'| \tag{A4}$$

corresponds to Fig. 23(d).

Similarly, we can obtain the following examples as shown in Fig. 23(e):

$$\rho_{\mu\beta} = \mathrm{tr}_{\alpha\nu} \rho, \tag{A5}$$

$$\rho_\beta = \mathrm{tr}_{\alpha\mu\nu} \rho, \tag{A6}$$

and especially,

$$\mathrm{tr}_{\alpha\beta\mu\nu} \rho = 1. \tag{A7}$$

[1] J. M. Maldacena, The large N limit of superconformal field theories and supergravity, Adv. Theor. Math. Phys. **2**, 231 (1998).

[2] S. S. Gubser, I. R. Klebanov, and A. M. Polyakov, Gauge theory correlators from noncritical string theory, Phys. Lett. B **428**, 105 (1998).

[3] E. Witten, Anti–de Sitter space and holography, Adv. Theor. Math. Phys. **2**, 253 (1998).

[4] S. Ryu and T. Takayanagi, Holographic derivation of entanglement entropy from AdS/CFT, Phys. Rev. Lett. **96**, 181602 (2006).

[5] S. Ryu and T. Takayanagi, Aspects of holographic entanglement entropy, J. High Energy Phys. 08 (2006) 045.

[6] V. E. Hubeny, M. Rangamani, and T. Takayanagi, A covariant holographic entanglement entropy proposal, J. High Energy Phys. 07 (2007) 062.

[7] G. Vidal, Entanglement renormalization, Phys. Rev. Lett. **99**, 220405 (2007).

[8] G. Vidal, Class of quantum many-body states that can be efficiently simulated, Phys. Rev. Lett. **101**, 110501 (2008).

[9] E. Glen and G. Vidal, Tensor network renormalization yields the multiscale entanglement renormalization ansatz, Phys. Rev. Lett. **115**, 200401 (2015).

[10] B. Swingle, Entanglement renormalization and holography, Phys. Rev. D **86**, 065007 (2012).

[11] B. Swingle, Constructing holographic spacetimes using entanglement renormalization, arXiv:1209.3304.

[12] F. Pastawski, B. Yoshida, D. Harlow, and J. Preskill, Holographic quantum error-correcting codes: Toy models for the bulk/boundary correspondence, J. High Energy Phys. 06 (2015) 149.

[13] P. Hayden, S. Nezami, X. L. Qi, N. Thomas, M. Walter, and Z. Yang, Holographic duality from random tensor networks, J. High Energy Phys. 11 (2016) 009.

[14] L. Chen, X. Liu, and L. Y. Hung, Emergent Einstein equation in p-adic conformal field theory tensor networks, Phys. Rev. Lett. **127**, 221602 (2021).

[15] L. Chen, X. Liu, and L. Y. Hung, Bending the Bruhat-Tits tree. Part II. The p-adic BTZ black hole and local diffeomorphism on the Bruhat-Tits tree, J. High Energy Phys. 09 (2021) 097.

[16] L. Chen, X. Liu, and L. Y. Hung, Bending the Bruhat-Tits tree. Part I. Tensor network and emergent Einstein equations, J. High Energy Phys. 06 (2021) 094.

[17] N. Bao, G. Penington, J. Sorce, and A. C. Wall, Beyond toy models: Distilling tensor networks in full AdS/CFT, J. High Energy Phys. 11 (2019) 069.

[18] N. Bao, G. Penington, J. Sorce, and A. C. Wall, Holographic tensor networks in full AdS/CFT, arXiv:1902.10157.

[19] J. Haegeman, T. J. Osborne, H. Verschelde, and F. Verstraete, Entanglement renormalization for quantum fields in real space, Phys. Rev. Lett. **110**, 100402 (2013).

[20] X. L. Qi, Exact holographic mapping and emergent spacetime geometry, arXiv:1309.6282.

[21] M. Miyaji, T. Numasawa, N. Shiba, T. Takayanagi, and K. Watanabe, Continuous multiscale entanglement renormalization ansatz as holographic surface-state correspondence, Phys. Rev. Lett. **115**, 171602 (2015).

[22] M. Miyaji and T. Takayanagi, Surface/state correspondence as a generalized holography, Prog. Theor. Exp. Phys. **2015**, 073B03 (2015).

[23] L. Chen, H. Zhang, H. C. Zhang, K. X. Ji, C. Shen, R. s. Wang, X. d. Zeng, and L. Y. Hung, Exact holographic tensor networks—constructing CFT_D from TQFT_{D+1}, arXiv:2210.12127.

[24] A. Almheiri, X. Dong, and D. Harlow, Bulk locality and quantum error correction in AdS/CFT, J. High Energy Phys. 04 (2015) 163.

[25] B. Czech, G. Evenbly, L. Lamprou, S. McCandlish, X. L. Qi, J. Sully, and G. Vidal, Tensor network quotient takes the vacuum to the thermal state, Phys. Rev. B **94**, 085101 (2016).

[26] G. Evenbly, Hyperinvariant tensor networks and holography, Phys. Rev. Lett. **119**, 141602 (2017).

[27] M. Steinberg, S. Feld, and A. Jahn, Holographic codes from hyperinvariant tensor networks, Nat. Commun. **14**, 7314 (2023).

[28] M. Steinberg and J. Prior, Conformal properties of hyperinvariant tensor networks, Sci. Rep. **12**, 532 (2022).

[29] B. Czech, P. H. Nguyen, and S. Swaminathan, A defect in holographic interpretations of tensor networks, J. High Energy Phys. 03 (2017) 090.

[30] S. Singh, N. A. McMahon, and G. K. Brennen, Holographic spin networks from tensor network states, Phys. Rev. D **97**, 026013 (2018).

[31] E. Colafranceschi and G. Adesso, Holographic entanglement in spin network states: A focused review, AVS Quantum Sci. **4**, 025901 (2022).

[32] G. Cheng, L. Chen, Z. C. Gu, and L. Y. Hung, Exact fixed-point tensor network construction for rational conformal field theory, arXiv:2311.18005.

[33] X. Zeng and L. Y. Hung, Bulk operator reconstruction in topological tensor network and generalized free fields, Entropy **25**, 1543 (2023).

[34] L. Y. Hung, W. Li, and C. M. Melby-Thompson, p-adic CFT is a holographic tensor network, J. High Energy Phys. 04 (2019) 170.

[35] A. Milsted and G. Vidal, Tensor networks as conformal transformations, arXiv:1805.12524.

[36] A. Milsted and G. Vidal, Tensor networks as path integral geometry, arXiv:1807.02501.

[37] A. Milsted and G. Vidal, Geometric interpretation of the multi-scale entanglement renormalization ansatz, arXiv:1812.00529.

[38] R. Sinai Kunkolienkar and K. Banerjee, Towards a dS/MERA correspondence, Int. J. Mod. Phys. D **26**, 1750143 (2017).

[39] N. Bao, C. Cao, S. M. Carroll, and A. Chatwin-Davies, De Sitter space as a tensor network: Cosmic no-hair, complementarity, and complexity, Phys. Rev. D **96**, 123536 (2017).

[40] C. Beny, Causal structure of the entanglement renormalization ansatz, New J. Phys. **15**, 023020 (2013).

[41] B. Czech, L. Lamprou, S. McCandlish, and J. Sully, Tensor networks from kinematic space, J. High Energy Phys. 07 (2016) 100.

[42] Y. Ling, Y. Xiao, and M. H. Wu, Note on quantum entanglement and quantum geometry, Phys. Lett. B **798**, 135023 (2019).
[43] Y. Ling, Y. Liu, Z. Y. Xian, and Y. Xiao, Tensor chain and constraints in tensor networks, J. High Energy Phys. 06 (2019) 032.
[44] Y. Ling, Y. Liu, Z. Y. Xian, and Y. Xiao, Quantum error correction and entanglement spectrum in tensor networks, Phys. Rev. D **99**, 026008 (2019).
[45] A. Bhattacharyya, L. Y. Hung, Y. Lei, and W. Li, Tensor network and (p-adic) AdS/CFT, J. High Energy Phys. 01 (2018) 139.
[46] A. Bhattacharyya, Z. S. Gao, L. Y. Hung, and S. N. Liu, Exploring the tensor networks/AdS correspondence, J. High Energy Phys. 08 (2016) 086.
[47] W. C. Gan and F. W. Shu, Holography as deep learning, Int. J. Mod. Phys. D **26**, 1743020 (2017).
[48] N. Bao, C. Cao, S. M. Carroll, A. Chatwin-Davies, N. Hunter-Jones, J. Pollack, and G. N. Remmen, Consistency conditions for an AdS multiscale entanglement renormalization ansatz correspondence, Phys. Rev. D **91**, 125036 (2015).
[49] C. Yu, F. Z. Chen, Y. Y. Lin, J. R. Sun, and Y. Sun, Note on surface growth approach for bulk reconstruction, Chin. Phys. C **46**, 085104 (2022).
[50] J. R. Sun and Y. Sun, On the emergence of gravitational dynamics from tensor networks, Commun. Theor. Phys. **75**, 085402 (2023).
[51] A. Belin, J. de Boer, D. L. Jafferis, P. Nayak, and J. Sonner, Approximate CFTs and random tensor models, arXiv:2308.03829.
[52] Y. Y. Lin, J. R. Sun, and Y. Sun, Surface growth scheme for bulk reconstruction and tensor network, J. High Energy Phys. 12 (2020) 083.
[53] M. Freedman and M. Headrick, Bit threads and holographic entanglement, Commun. Math. Phys. **352**, 407 (2017).
[54] S. X. Cui, P. Hayden, T. He, M. Headrick, B. Stoica, and M. Walter, Bit threads and holographic monogamy, Commun. Math. Phys. **376**, 609 (2019).
[55] M. Headrick and V. E. Hubeny, Riemannian and Lorentzian flow-cut theorems, Classical Quantum Gravity **35**, 10 (2018).
[56] M. Headrick and V. E. Hubeny, Covariant bit threads, J. High Energy Phys. 07 (2023) 180.
[57] M. Headrick, J. Held, and J. Herman, Crossing versus locking: Bit threads and continuum multiflows, Commun. Math. Phys. **396**, 265 (2022).
[58] Y. Y. Lin, J. R. Sun, and Y. Sun, Bit thread, entanglement distillation, and entanglement of purification, Phys. Rev. D **103**, 126002 (2021).
[59] Y. Y. Lin, J. R. Sun, and J. Zhang, Deriving the PEE proposal from the locking bit thread configuration, J. High Energy Phys. 10 (2021) 164.
[60] Y. Y. Lin, J. R. Sun, Y. Sun, and J. C. Jin, The PEE aspects of entanglement islands from bit threads, J. High Energy Phys. 07 (2022) 009.
[61] Y. Y. Lin and J. C. Jin, Thread/state correspondence: From bit threads to qubit threads, J. High Energy Phys. 02 (2023) 245.
[62] Y. Y. Lin and J. C. Jin, Thread/state correspondence: The qubit threads model of holographic gravity, arXiv:2208.08963.
[63] Y. Y. Lin, Distilled density matrices of holographic partial entanglement entropy from thread-state correspondence, Phys. Rev. D **108**, 106010 (2023).
[64] J. Kudler-Flam, I. MacCormack, and S. Ryu, Holographic entanglement contour, bit threads, and the entanglement tsunami, J. Phys. A **52**, 325401 (2019).
[65] A. Rolph, Local measures of entanglement in black holes and CFTs, SciPost Phys. **12**, 079 (2022).
[66] J. Harper, Perfect tensor hyperthreads, J. High Energy Phys. 09 (2022) 239.
[67] J. Harper, Hyperthreads in holographic spacetimes, J. High Energy Phys. 09 (2021) 118.
[68] J. Lin, Y. Lu, and Q. Wen, Geometrizing the partial entanglement entropy: From PEE threads to bit threads, J. High Energy Phys. 02 (2024) 191.
[69] C. A. Agón and J. F. Pedraza, Quantum bit threads and holographic entanglement, J. High Energy Phys. 02 (2022) 180.
[70] A. Rolph, Quantum bit threads, SciPost Phys. **14**, 097 (2023).
[71] C. B. Chen, F. W. Shu, and M. H. Wu, Quantum bit threads of MERA tensor network in large c limit, Chin. Phys. C **44**, 075102 (2020).
[72] V. E. Hubeny, Bulk locality and cooperative flows, J. High Energy Phys. 12 (2018) 068.
[73] C. A. Agón, J. De Boer, and J. F. Pedraza, Geometric aspects of holographic bit threads, J. High Energy Phys. 05 (2019) 075.
[74] D. H. Du, C. B. Chen, and F. W. Shu, Bit threads and holographic entanglement of purification, J. High Energy Phys. 08 (2019) 140.
[75] N. Bao, A. Chatwin-Davies, J. Pollack, and G. N. Remmen, Towards a bit threads derivation of holographic entanglement of purification, J. High Energy Phys. 07 (2019) 152.
[76] J. Harper and M. Headrick, Bit threads and holographic entanglement of purification, J. High Energy Phys. 08 (2019) 101.
[77] C. A. Agón and M. Mezei, Bit threads and the membrane theory of entanglement dynamics, J. High Energy Phys. 11 (2021) 167.
[78] D. H. Du, F. W. Shu, and K. X. Zhu, Inequalities of holographic entanglement of purification from bit threads, Eur. Phys. J. C **80**, 700 (2020).
[79] C. A. Agón, E. Cáceres, and J. F. Pedraza, Bit threads, Einstein's equations and bulk locality, J. High Energy Phys. 01 (2021) 193.
[80] N. Bao and J. Harper, Bit threads on hypergraphs, arXiv:2012.07872.
[81] J. F. Pedraza, A. Russo, A. Svesko, and Z. Weller-Davies, Sewing spacetime with Lorentzian threads: Complexity and the emergence of time in quantum gravity, J. High Energy Phys. 02 (2022) 093.
[82] J. F. Pedraza, A. Russo, A. Svesko, and Z. Weller-Davies, Lorentzian threads as gatelines and holographic complexity, Phys. Rev. Lett. **127**, 271602 (2021).
[83] J. Harper, M. Headrick, and A. Rolph, Bit threads in higher curvature gravity, J. High Energy Phys. 11 (2018) 168.

[84] E. Shaghoulian and L. Susskind, Entanglement in de Sitter space, J. High Energy Phys. 08 (2022) 198.
[85] L. Susskind, Entanglement and chaos in de Sitter space holography: An SYK example, J. High Energy Astrophys. **1**, 1 (2021).
[86] I. Bakhmatov, N. S. Deger, J. Gutowski, E. Ó. Colgáin, and H. Yavartanoo, Calibrated entanglement entropy, J. High Energy Phys. 07 (2017) 117.
[87] B. Czech, L. Lamprou, S. McCandlish, and J. Sully, Integral geometry and holography, J. High Energy Phys. 10 (2015) 175.
[88] N. Bao, S. Nezami, H. Ooguri, B. Stoica, J. Sully, and M. Walter, The holographic entropy cone, J. High Energy Phys. 09 (2015) 130.
[89] V. E. Hubeny, M. Rangamani, and M. Rota, The holographic entropy arrangement, Fortschr. Phys. **67**, 1900011 (2019).
[90] V. E. Hubeny, M. Rangamani, and M. Rota, Holographic entropy relations, Fortschr. Phys. **66**, no. 11–12, 1800067 (2018).
[91] S. Hernández Cuenca, Holographic entropy cone for five regions, Phys. Rev. D **100**, 026004 (2019).
[92] G. Vidal and Y. Chen, Entanglement contour, J. Stat. Mech. (2014) P10011.
[93] Q. Wen, Formulas for partial entanglement entropy, Phys. Rev. Res. **2**, 023170 (2020).
[94] Q. Wen, Fine structure in holographic entanglement and entanglement contour, Phys. Rev. D **98**, 106004 (2018).
[95] Q. Wen, Entanglement contour and modular flow from subset entanglement entropies, J. High Energy Phys. 05 (2020) 018.
[96] M. Han and Q. Wen, Entanglement entropy from entanglement contour: Higher dimensions, SciPost Phys. Core **5**, 020 (2022).
[97] P. Nguyen, T. Devakul, M. G. Halbasch, M. P. Zaletel, and B. Swingle, Entanglement of purification: From spin chains to holography, J. High Energy Phys. 01 (2018) 098.
[98] T. Takayanagi and K. Umemoto, Entanglement of purification through holographic duality, Nat. Phys. **14**, 573 (2018).
[99] Q. Wen, Balanced partial entanglement and the entanglement wedge cross section, J. High Energy Phys. 04 (2021) 301.
[100] H. A. Camargo, P. Nandy, Q. Wen, and H. Zhong, Balanced partial entanglement and mixed state correlations, SciPost Phys. **12**, 137 (2022).
[101] Q. Wen and H. Zhong, Covariant entanglement wedge cross-section, balanced partial entanglement and gravitational anomalies, SciPost Phys. **13**, 056 (2022).
[102] W. Helwig, W. Cui, A. Riera, J. I. Latorre, and H. K. Lo, Absolute maximal entanglement and quantum secret sharing, Phys. Rev. A **86**, 052335 (2012).
[103] W. Helwig, Absolutely maximally entangled qudit graph states, arXiv:1306.2879.
[104] S. Dutta and T. Faulkner, A canonical purification for the entanglement wedge cross-section, J. High Energy Phys. 03 (2021) 178.
[105] J. Kudler-Flam and S. Ryu, Entanglement negativity and minimal entanglement wedge cross sections in holographic theories, Phys. Rev. D **99**, 106014 (2019).
[106] Y. Kusuki, J. Kudler-Flam, and S. Ryu, Derivation of holographic negativity in AdS_3/CFT_2, Phys. Rev. Lett. **123**, 131603 (2019).
[107] K. Tamaoka, Entanglement wedge cross section from the dual density matrix, Phys. Rev. Lett. **122**, 141601 (2019).
[108] R. Espíndola, A. Guijosa, and J. F. Pedraza, Entanglement wedge reconstruction and entanglement of purification, Eur. Phys. J. C **78**, 646 (2018).
[109] M. Nozaki, T. Numasawa, and T. Takayanagi, Holographic local quenches and entanglement density, J. High Energy Phys. 05 (2013) 080.
[110] N. Bao, A. Chatwin-Davies, and G. N. Remmen, Entanglement of purification and multiboundary wormhole geometries, J. High Energy Phys. 02 (2019) 110.
[111] N. Bao, Minimal purifications, wormhole geometries, and the complexity = action proposal, arXiv:1811.03113.
[112] B. Czech, J. L. Karczmarek, F. Nogueira, and M. Van Raamsdonk, The gravity dual of a density matrix, Classical Quantum Gravity **29**, 155009 (2012).
[113] M. Headrick, V. E. Hubeny, A. Lawrence, and M. Rangamani, Causality & holographic entanglement entropy, J. High Energy Phys. 12 (2014) 162.
[114] A. C. Wall, Maximin surfaces, and the strong subadditivity of the covariant holographic entanglement entropy, Classical Quantum Gravity **31**, 225007 (2014).
[115] D. L. Jafferis, A. Lewkowycz, J. Maldacena, and S. J. Suh, Relative entropy equals bulk relative entropy, J. High Energy Phys. 06 (2016) 004.
[116] X. Dong, D. Harlow, and A. C. Wall, Reconstruction of bulk operators within the entanglement wedge in gauge-gravity duality, Phys. Rev. Lett. **117**, 021601 (2016).
[117] J. Cotler, P. Hayden, G. Penington, G. Salton, B. Swingle, and M. Walter, Entanglement wedge reconstruction via universal recovery channels, Phys. Rev. X **9**, 031011 (2019).
[118] Y. Y. Lin and J. Zhang, Holographic thread picture, quantum circuit and canonical entanglement distillation (to be published).
[119] V. Balasubramanian, B. Czech, B. D. Chowdhury, and J. de Boer, The entropy of a hole in spacetime, J. High Energy Phys. 10 (2013) 220.
[120] V. Balasubramanian, B. D. Chowdhury, B. Czech, J. de Boer, and M. P. Heller, Bulk curves from boundary data in holography, Phys. Rev. D **89**, 086004 (2014).
[121] B. Czech and L. Lamprou, Holographic definition of points and distances, Phys. Rev. D **90**, 106005 (2014).
[122] M. Banados, C. Teitelboim, and J. Zanelli, The black hole in three-dimensional space-time, Phys. Rev. Lett. **69**, 1849 (1992).
[123] W. C. Gan, F. W. Shu, and M. H. Wu, Emergent geometry, thermal CFT and surface/state correspondence, Phys. Lett. B **772**, 464 (2017).